PERGAMON

Journal of Structural Geology 21 (1999) 1575–1601

JOURNAL OF STRUCTURAL GEOLOGY

www.elsevier.nl/locate/jstrugeo

Structural analysis of a complex nappe sequence and late-orogenic basins from the Aegean Island of Samos, Greece

Uwe Ring*, Susanne Laws [1], Matthias Bernet [2]

Institut für Geowissenschaften, Johannes Gutenberg-Universität, 55099 Mainz, Germany

Received 20 January 1998; accepted 18 March 1999

Abstract

The island of Samos in the Aegean Sea exposes high-pressure metamorphic rocks of the Cycladic blueschist unit which are sandwiched between the mildly blueschist-facies Kerketas nappe below and the overlying non-metamorphic Kallithea nappe. Structural and metamorphic analysis shows that deformation can generally be divided into four main stages: (1) Eocene and earliest Oligocene ~ESE–WNW-oriented nappe stacking (D_1 and D_2) associated with blueschist- and transitional blueschist–greenschist-facies metamorphism (M_1 and M_2). D_2 caused emplacement of the blueschist unit onto the Kerketas nappe indicating that thrusting occurred during decompression. (2) A subsequent history of Oligocene and Miocene horizontal crustal extension (D_3) before and after greenschist-facies metamorphism (M_3). Ductile flow during D_3 was characterized by a high degree of coaxial deformation but in general caused displacement of upper units towards the ENE. Nonetheless, the late-stage D_3 emplacement of the Kallithea nappe between 9 and 10 Ma had a top-to-the-NW/NNW sense of shear. (3) A short period of brittle E–W crustal contraction (D_4) occurred between <8.6 and ~9 Ma. (4) A phase of N–S-directed normal faulting (D_5, <8.6 Ma to Recent). ESE–WNW-directed tectonic transport during D_1 through D_3 is in contrast to uniform NNE–SSW-directed tectonic transport in the adjacent Cyclades, Greece, as well as in the neighbouring Menderes Massif of western Turkey. Published paleomagnetic data reveal sinistral rotation between the Cyclades and western Turkey. We interpret this rotation as a consequence of differential extension between the severely extended Aegean and the moderately extended Menderes Massif during D_3. The onset of D_3 crustal extension is coeval with a marked change in the thermal structure. We propose that the thermal reorganization was associated with the retreat of the subduction zone towards the external Hellenides in the Early Oligocene and a subsequent increase in magmatic activity.

1. Introduction

Research over the last two decades revealed the importance of NNE–SSW-directed horizontal crustal extension in the Aegean (e.g. Le Pichon and Angelier, 1979; Lister et al., 1984; Avigad and Garfunkel, 1991) and the adjacent Menderes Massif of western Turkey (e.g. Hetzel et al., 1995). Eocene blueschist-facies rocks of the Cycladic blueschist unit are envisioned as having been dragged to the surface in the footwall of major crustal shear zones to form the Aegean metamorphic core complexes (Lister et al., 1984). However, no Tertiary high-pressure rocks have been reported so far from the base of the metamorphic core complex of the central Menderes Massif (Ring et al., 1999). Differential extension between the Aegean and the Menderes Massif is indicated by the fact that the Aegean, especially the Cretan Sea, is underlain by intensely attenuated continental crust whereas the Menderes Massif is not (Makris and Stobbe, 1984). The island of Samos is located between these differently extending areas in the Aegean and the Menderes Massif and the structural evolution of Samos might have been controlled to some degree by differential extension. Paleomagnetic data from Lesbos Island and

* Corresponding author.
E-mail address: ring@mail.uni-mainz.de (U. Ring)
[1] Current address: Institut für Ingenieurgeologie, ETH Hönggerberg, 8093 Zürich, Switzerland.
[2] Current address: Department of Geology and Geophysics, Yale University, New Haven, CT 06520-8109, USA.

0191-8141/99/$ - see front matter
PII: S0191-8141(99)00108-X

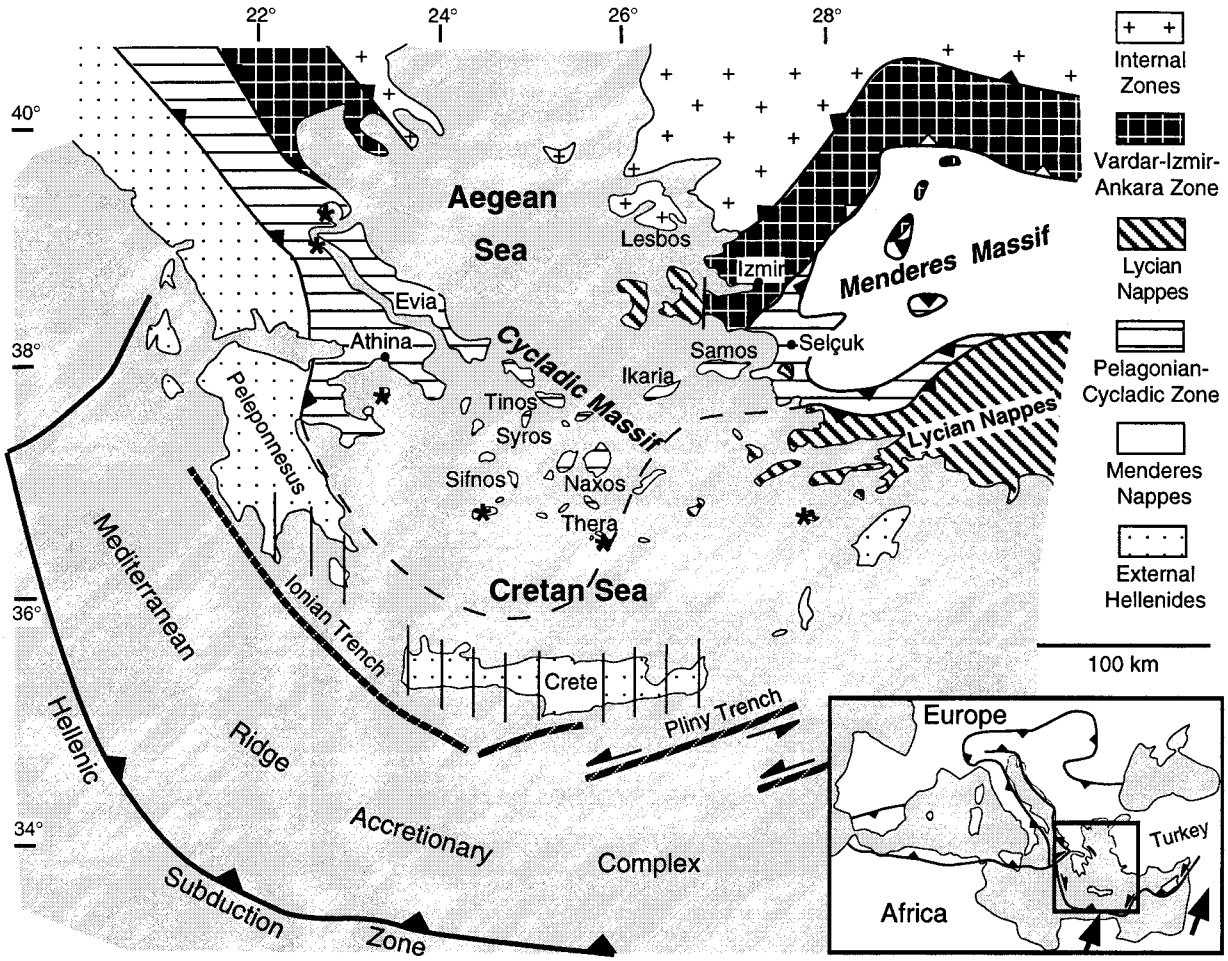

Fig. 1. Generalized tectonic map of the Aegean and adjacent mainlands (greatly modified from Jacobshagen, 1986 and Le Pichon et al., 1995) showing major tectonic units and present-day Hellenic subduction zone north of the Libyan coast. The Pelagonian–Cycladic zones, which have been joined together here, and the Vardar–Izmir–Ankara zones form high-pressure belts of Cretaceous to Early Tertiary age which span a wide area from the Greek mainland across the northern Aegean Sea into Turkey. Miocene high-pressure rocks (vertically ruled pattern, Theye et al., 1992) occupy a more restricted area than the older high-pressure rocks and occur to the south/southeast of the Late Pliocene to Recent volcanic arc delineated by calc-alkaline volcanoes (asterisks). Inset: Miocene to Recent thrust fronts in the Mediterranean region and location of main map; arrows show the integrated relative motion of Africa with respect to Europe from 35 Ma to present in the eastern Mediterranean.

the Izmir region (Kissel and Laj, 1988) (Fig. 1) shows an abrupt switch from slight clockwise rotation (6°) on Lesbos Island to pronounced anticlockwise rotation (~30°) in westernmost Turkey. The age of this rotation is not precisely known but Middle Miocene appears most reasonable (Kissel and Laj, 1988).

The pre-extension emplacement of the Cycladic blueschist unit is poorly understood due, at least in part, to the fact that the deep tectonic units onto which the blueschists have been emplaced are not exposed on most Aegean islands. In this regard the island of Samos (Figs. 1 and 2) in the easternmost Aegean Sea is of particular interest because it exposes the Kerketas nappe of the external Hellenides which occurs structurally below the Cycladic blueschist unit.

In this contribution, we analyse the structural evolution and its relationship to the metamorphic history of the nappe pile and its Neogene cover on Samos Island in order to decipher the roles of crustal contraction and crustal extension. The manifold problems in trying to relate a particular phase of deformation to crustal shortening or lengthening have been pointed out recently by a number of studies (Ring and Brandon, 1994; Wheeler and Butler, 1994; Ring, 1995). Then we discuss the tectonometamorphic history of Samos within the framework of Aegean tectonics.

2. Regional setting

The Cycladic Massif consists of a pile of nappes (Altherr and Seidel, 1977) (Fig. 3). In ascending order the major tectonic units are: (1) The Basal unit as part of the external Hellenides. (2) The Cycladic blueschist

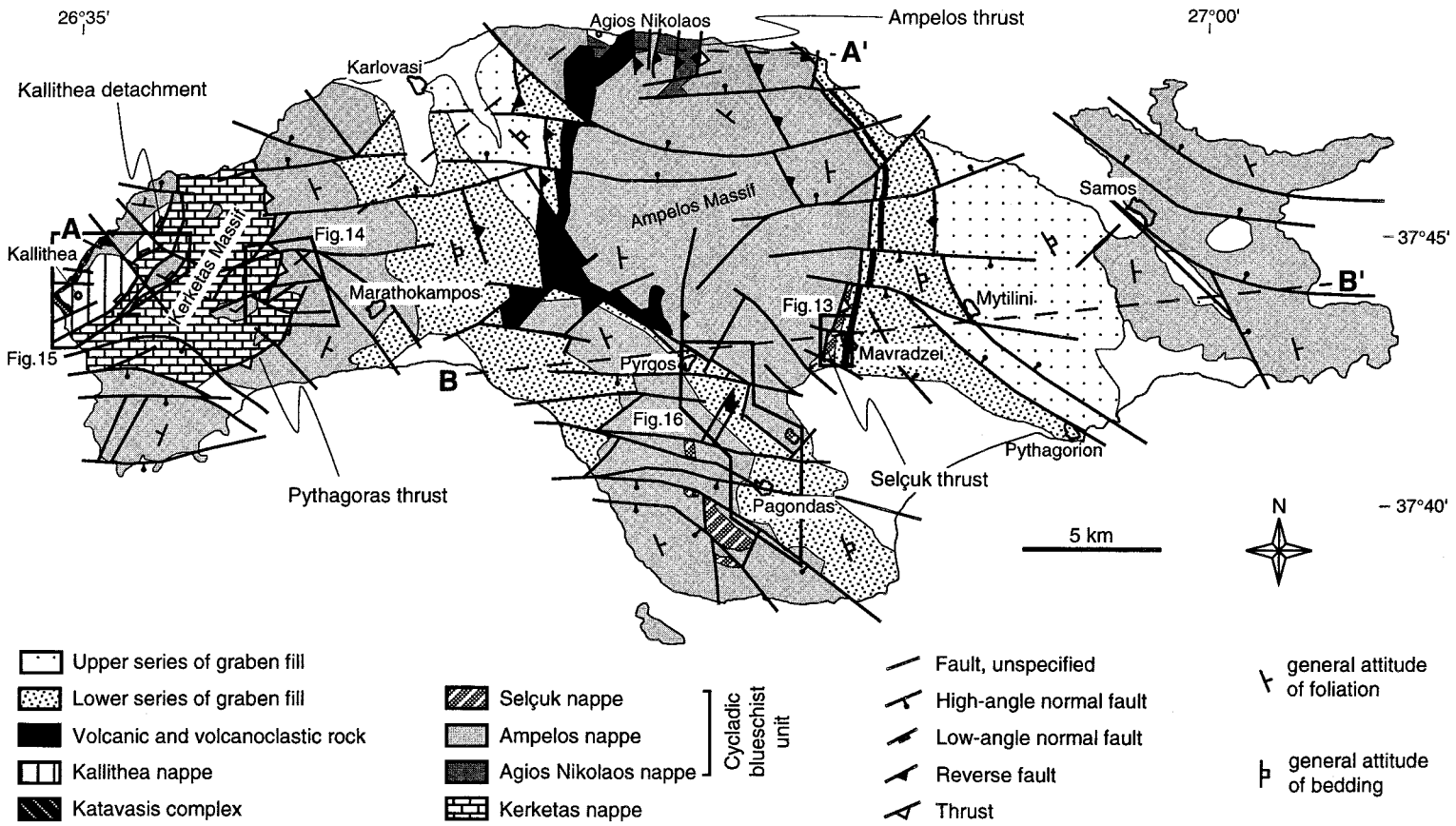

Fig. 2. Simplified geologic and tectonic map of Samos Island showing major rock units, thrusts and faults (with barbs and ticks on the hanging wall sides) and representative structural attitudes of rocks. The different nappes are described in Table 1. Lower series of graben fill comprise Basal Conglomerate, Pythagorion and Hora Formations; Upper series of graben fill include Mytilini and Kokkarion Formations (see also Figs. 3 and 4 and Table 2). The D_1 Ampelos and Selçuk thrusts are the basal thrusts of the Ampelos and Selçuk nappes, respectively. The D_2 Pythagoras thrust put the Cycladic blueschist unit on top of the Kerketas nappe (the Pythagoras thrust is named after 'Pythagoras Cave' c. 50 m above the thrust plane west of Marathokampos). The Kallithea detachment is a late-D_3 low-angle extensional fault. Widespread Middle and mainly Late Miocene volcanic and volcanoclastic rocks occur at the eastern and northeastern margin of the Karlovasi and Pyrgos graben. Subordinate volcanics also occur at the western side of the Mytilini basin. Numerous reverse (D_4) and normal (D_5) faults overprinted all earlier ductile contacts. We interpret the curved D_5 high-angle normal faults to have a listric geometry. Positions of cross-sections A–A′ and B–B′ (Fig. 4) and locations of maps shown in Figs. 13–16 are indicated.

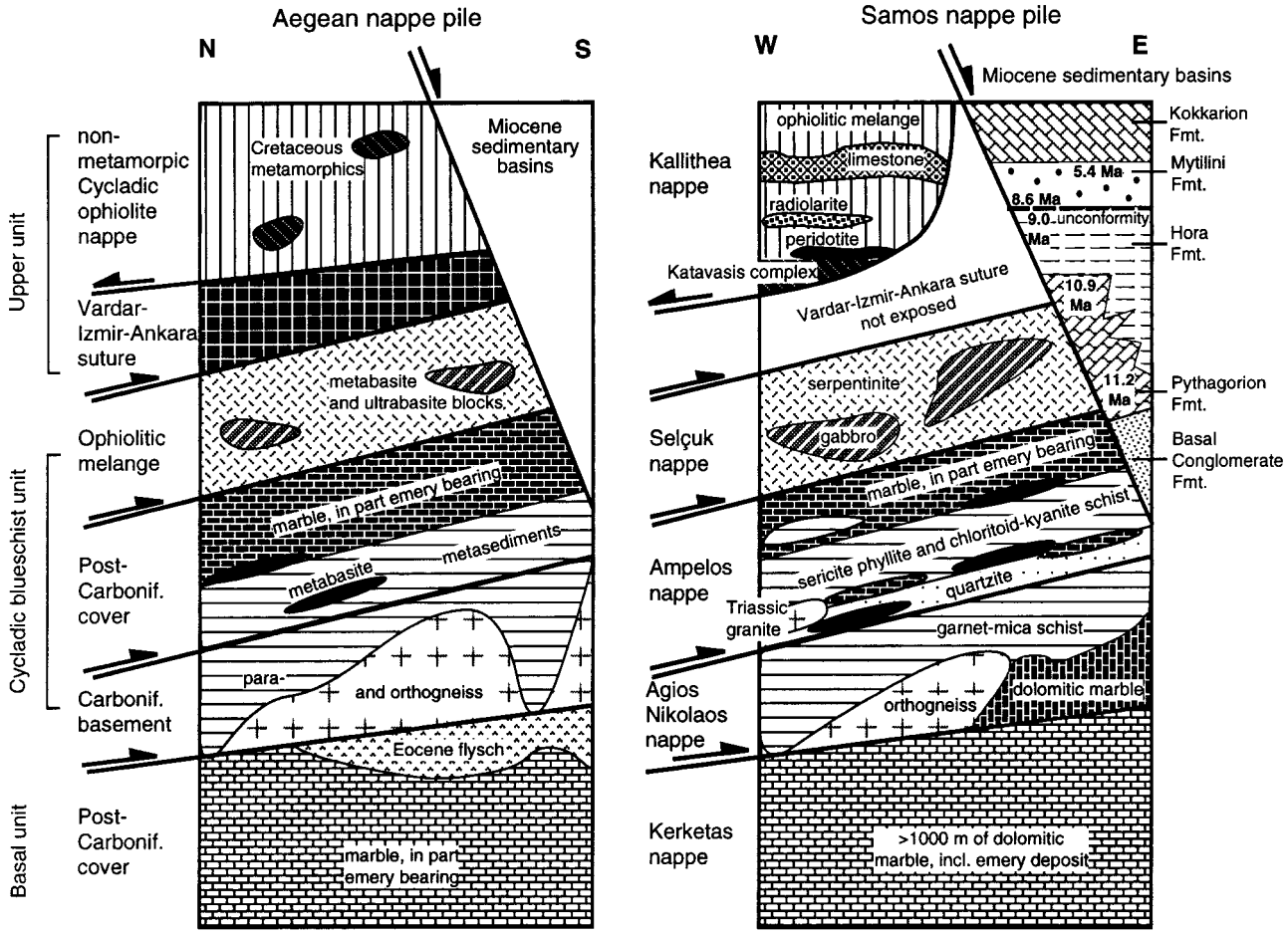

Fig. 3. Idealized comparative tectonostratigraphic columns of the nappe piles in the Aegean and on Samos Island. Ar/Ar age data of Weidmann et al. (1984) provide age constraints for sedimentary rocks in Miocene basins.

unit comprising at least three separate members: (i) A Carboniferous basement nappe, overlain by (ii) a nappe made up of a probably post-Carboniferous shelf sequence (Altherr and Seidel, 1977). (iii) Above this shelf sequence occurs a melange-like nappe of ophiolitic rocks embedded in a serpentinitic and metapelitic matrix (Okrusch and Bröcker, 1990; Erdogan and Güngör, 1992; Candan et al., 1997). (3) The Upper unit consists of three subunits: (i) The Lycian nappes which are capped by Eocene to Oligocene clastic rocks (Okay, 1989; Collins and Robertson, 1998). (ii) The Cretaceous to Paleogene Vardar–Izmir–Ankara suture zone which fringes the Cycladic and the Menderes Massif to the north. (iii) The non-metamorphic composite Cycladic ophiolite nappe, which contains tectonically intercalated low-pressure metamorphic rocks of Cretaceous age (Reinecke, 1982). (4) Sedimentary basins filled with Miocene and younger sediments. These basins formed at 13 ± 5 Ma (Le Pichon and Angelier, 1979).

Both the Cycladic and the Menderes Massif have been the site of late-orogenic crustal extension. It has been suggested that extension started in the latest Oligocene (Seyitoglu et al., 1992; Gautier et al., 1993) or already in the Early Oligocene (Raouzaios et al., 1996). Crustal extension in the Cycladic Massif is generally considered to be the result of the retreat of the Hellenic slab (Lister et al., 1984; Buick, 1991) and occurred and still occurs in the fore-arc high (Crete; Fassoulas et al., 1994; Thomson et al., 1999) in the arc (on the island of Thera; Lister and Forster, 1996) and in the back-arc region (Cycladic Massif; Lister et al., 1984; Gautier et al., 1993).

3. Geology of Samos

Our mapping at the 1:10 000 scale over the last four years covered approximately 50% of Samos Island (Fig. 2) and augmented the work of Theodoropoulos (1979) and Papanikolaou (1979). The general structure is dominated by numerous late faults. A major, N-dipping normal fault occurs just north of the island and it tilted Samos Island to the south. Cross-sections

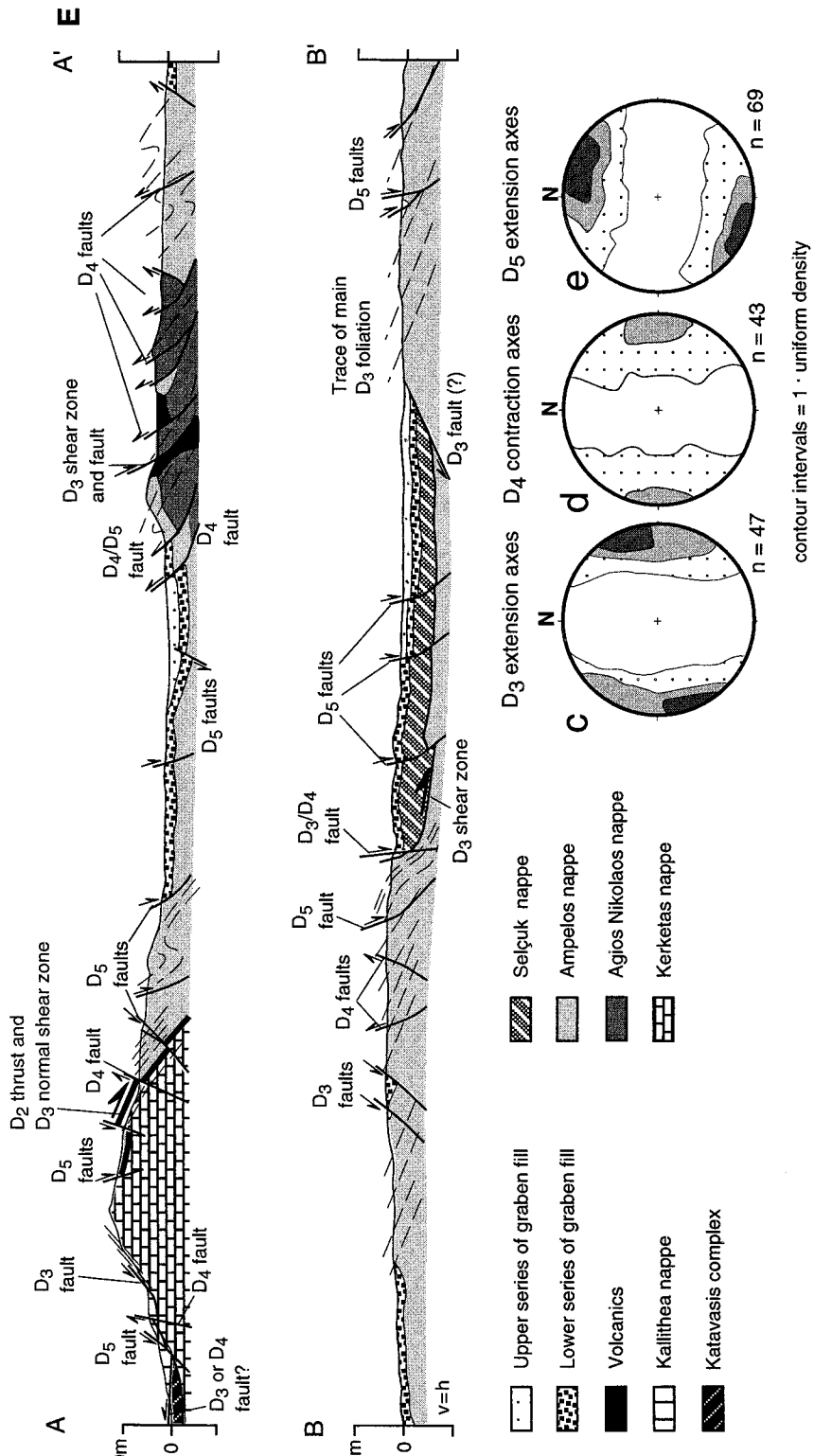

Fig. 4. (a) and (b) Serial cross-sections A–A′ and B–B′ through Samos Island showing general architecture of the island (refer to Fig. 2 for transect positions). The trace of the main foliation illustrates the generally E-dipping structure (see also Fig. 5). (c–e) Summary plots of contraction and extension axes as deduced from fault-slip analysis of D_3, D_4 and D_5 faults.

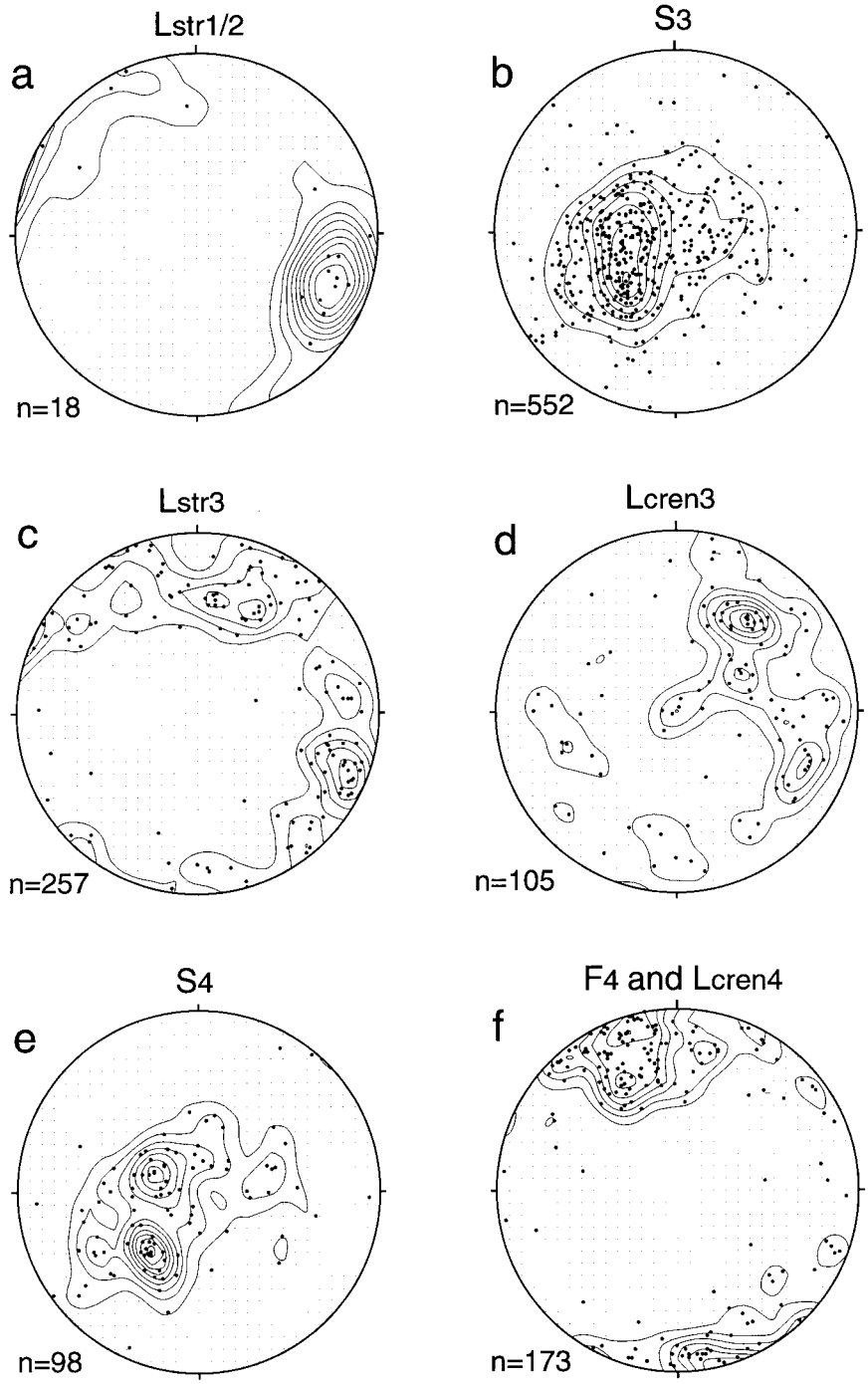

Fig. 5. Orientational data (lower-hemisphere equal-area projections). (a) $L_{str1/2}$; (b) S_3; (c) L_{str3}; (d) L_{cren3}; (e) S_4; (f) L_{cren4} and F_4 axes.

(Fig. 4) and orientation data (Fig. 5) show that the nappe pile dips to the east. This nappe pile is described in Table 1.

The final emplacement of the non-metamorphic Cycladic ophiolite nappe (Kallithea nappe in Samos) above the blueschist unit is generally regarded to be due to horizontal crustal extension (e.g. Böger, 1983; Lister et al., 1984). Böger (1983) suggests a generalized age of 8–10 Ma for nappe emplacement across the entire Aegean. West of Kallithea (Fig. 2), the Katavasis complex is in fault contact with the Kallithea nappe (Fig. 4). Mezger and Okrusch (1985) speculated that the Katavasis complex belongs to the Cretaceous high-temperature rocks, which form crystalline slices within the Cycladic ophiolite nappe. If so, the Katavasis complex would belong tectonically to the Kallithea nappe. We will return to this problem below.

Table 1
Geology of the nappes of Samos Island

Nappes	Regional tectonic unit	Cretaceous and Tertiary metamorphism	Comments
Kallithea nappe (uppermost nappe)	Composite Cycladic ophiolite nappe	Non-metamorphic	Chaotic brittle disruption; melange-like internal structure
Katavasis complex	Composite Cycladic ophiolite nappe[a]	Upper amphibolite facies (no Tertiary blueschist-facies overprint)[b]	At ~10 Ma intruded by up to ~10 m thick igneous dikes[b]; dikes do not intrude directly overlying Kallithea nappe
Selçuk nappe	Cycladic blueschist unit (ophiolitic melange)	Blueschist facies followed by greenschist facies overprint[c]	Resembles metabasite association of Syros Island[d]
Ampelos nappe	Cycladic blueschist unit (post-Carboniferous cover nappe)	Blueschist facies followed by greenschist facies overprint[c]	Two augengneiss slices in lower part yielded Pb/Pb zircon ages of 230–240 Ma[e]
Agios Nikolaos nappe	Cycladic blueschist unit (Carboniferous basement nappe)	Blueschist facies followed by greenschist facies overprint[c]	Orthogneiss sample yielded Pb/Pb zircon age of 302 Ma[f]; Carboniferous amphibolite-facies metamorphic relics
Kerketas nappe (lowermost nappe in Samos)	Basal unit	Incipient high-pressure metamorphism followed by greenschist facies overprint[c]	>1500 m thick sequence of monotonous dolmitic marble

[a] See discussion in text.
[b] Mezger and Okrusch (1985).
[c] For details see Table 3.
[d] Okrusch and Bröcker (1990).
[e] T. Reischmann (personal communication, 1997).
[f] M. Engel (personal communication, 1997).

The Karlovasi, Pyrgos and Mytilini graben are filled with Miocene/Pliocene fluviatile and lacustrine sediments (Table 2, Fig. 3). Above the Basal Conglomerate Formation follow the Pythagorion and Hora Formations. Both formations also laterally interfinger with each other. The sediments of the Hora Formation are thought to have formed in a deeper basin than the limestone of the Pythagorion Formation (Weidmann et al., 1984). A major angular unconformity occurs on top of the Hora Formation. Lacustrine sedimentation is succeeded by fluviatile conglomerate of the basal Mytilini Formation (Old Mill Beds sensu Weidmann et al., 1984). Weidmann (1984, fig. 6, p. 486) showed that in some places the unconformity occurs on top of the Old Mill Beds, whereas in other places it occurs below the Old Mill Beds. This difference might indicate that the unconformity did not occur at the same time in all parts of the basin or it

Table 2
Neogene basins on Samos Island

Formation[a]	General lithology	Distinct sedimentologic features	Stratigraphic age[b]
Kokkarion Formation	Porous lacustrine limestone, tuffaceous marl and silt	Erosional surface at top	Zanclean
Mytilini Formation	Conglomerate, sandstone, siltstone, tuffaceous marl, paleosol, channel-fill deposits, chalky lacustrine limestone, tuffaceous marl and sand at top	Contains pebbles of volcanic rocks, Cycladic blueschist unit and Kerketas nappe	Late Tortonian and Messinian
Hora Formation	Thick-bedded limestone, thin-bedded marl, tuff	>400 m thick; marls contain abundant slump folds; deep lacustrine deposition[a]; pronounced unconformity on top	Early Tortonian
Pythagorion Formation	Thick-bedded lacustrine limestone, locally silt, gravel and tuff	Desiccation cracks, wave ripples and bioturbation features attest to shallow lacustrine deposition	Early Tortonian
Basal Conglomerate Formation	Poorly sorted angular cobble, conglomerate, rare thin tuff intercalations	Contains clasts of Agios Nikolaos, Ampelos and Selçuk nappes	Serravallian

[a] According to Weidmann et al. (1984).
[b] For radiometric age data from tuff horizons see Weidmann et al. (1984) and Fig. 3.

might indicate that the Old Mill Beds are time-transgressive.

4. Metamorphic history

The *P–T* conditions for high-pressure metamorphism (Table 3, Fig. 6) reveal mildly blueschist-facies conditions in the Kerketas nappe and a pronounced metamorphic break (up to 10 kbar) towards higher pressures and temperatures above the Kerketas nappe. Within the Cycladic blueschist unit, maximum metamorphic conditions decreased structurally upward. As will be shown below, maximum high-pressure assemblages in the Cycladic blueschist unit developed during the first deformational event (D_1) and are therefore referred to as M_1. The associated S_1 foliation was porphyroblastically overgrown by glaucophane, chloritoid and kyanite during a static growth event (Fig. 7a). Maximum pressure in the Kerketas nappe occurred during the D_2 deformation and therefore the mildly blueschist-facies event in the Kerketas nappe is regarded as M_2 (Table 3). During D_2, the M_1 high-pressure assemblages in the Cycladic blueschist unit were replaced by M_2 transitional blueschist–greenschist-facies assemblages.

A subsequent Barrovian-type metamorphic overprint (M_3) was characterized by the prograde formation of garnet and more rarely by biotite in metapelite of the Agios Nikolaos and Ampelos nappes (Chen, 1995). Chen et al. (1995) estimated about 6–7 kbar and 450–490°C for M_3 with slightly higher temperatures in the western than in the eastern part of the island. The data show that M_3 occurred during further decompression but increasing temperature (Table 3).

Age data for the Cycladic blueschist unit for a number of islands (e.g. Sifnos, Naxos, Ios, Syros, Tinos, Ikaria) across the entire Aegean are remarkably similar and are interpreted to date the peak of high-pressure metamorphism at ⩾50 Ma. Cooling below ~350–450°C (assumed phengite closure temperature) took place between 35 and 40 Ma and the Barrovian-type overprint occurred at about 18–25 Ma (Altherr et al., 1982; Wijbrans and McDougall, 1988; Wijbrans et al., 1990; Bröcker et al., 1993; Bröcker and Enders, 1999) (Fig. 6) concurrent with and followed by calc-alkaline magmatism. Unpublished K/Ar age data on white mica from Samos Island by H. Kreuzer are interpreted to agree with this age pattern (Chen et al., 1995).

5. Deformation history

Detailed structural studies were conducted at the tectonic contacts between the various tectonostratigraphic units and within the Agios Nikolaos, Ampelos and Kallithea nappes and the Neogene graben sediments. Based mainly on microstructural relations of mineral parageneses and overprinting criteria, we recognized sets of structures formed during five major deformational events (D_1–D_5). In general, D_3 is the dominant ductile deformation. Earlier structures and fabrics have been substantially modified and transposed and therefore only a little information about the

Table 3
Metamorphic data

Nappe	Metamorphic event	Lithology and mineral assemblages[a]	*P–T* conditions
Selçuk nappe	M_1	Metabasite: omp + zo + ep_1[b] and gl_1 + ep_1 + $phen_1$ + ab_1 + chl_1 + sph + rt + hem + cc[c]	400–470°C, 10–14 kbar
Ampelos nappe	M_1	Metabasite: gl_1 + ep_1 + $phen_1$ + chl_1 + ab_1 + sph + rt + hem + cc[d]	420–490°C, 11–13 kbar[d]
		Metapelite: qtz_1 + gl_1 + $phen_1$ + par_1 + chl_1 + ctd_1 + ky_1 + ab_1 + car + tur[cdef]	~ 500°C, ~15 kbar[f]
	M_3	Metapelite: bt + $phen_3$ + chl_3 + ab_3 + ep_3	450–490°C, 6–7 kbar[d]
Agios Nikolaos nappe	M_1	Metabasite: gl_1 + ep_1 + grt_1 + $phen_1$ + par_1 + chl_1 + ab_1 + clz + sph + rt + hem + cc[d]	500–550°C, > 12 kbar[d]
		Metapelite: qtz_1 + gl_1 + ep_1 + grt_1 + $phen_1$ + par_1 + chl_1 + ctd_1 + ab_1 + sph + rt + hem[d]	520–530°C, ~19 kbar[f]
	M_2	Metapelite: qtz_2 + $phen_2$ + par_2 + chl_2 + ep_2 + ab_2	380–420°C, 7–8 kbar
		Metabasite: calc. amph + chl_2 + par_2 + pl_2[f]	420–450°C, 9.5–10 kbar[f]
	M_3	Metapelite: grt_3 + bt + $phen_3$ + chl_3 + ab_3 + ep_3[d]	450–490°C, 6–7 kbar[e]
Kerketas nappe	M_2	Impure marble: qtz + phen + par + chl + tlc + dol + cc	350–400°C, 7–10 kbar
	M_3	Metabauxite: crn + hem + ilm + spl + rt[g]	~ 450°C, 4–6 kbar[g]

[a] Mineral abbreviations after Kretz (1983).
[b] Mposkos and Perdikatsis (1984).
[c] Okrusch et al. (1984).
[d] Chen (1995).
[e] Chen et al. (l995).
[f] Will et al. (1998).
[g] Mposkos (1978).

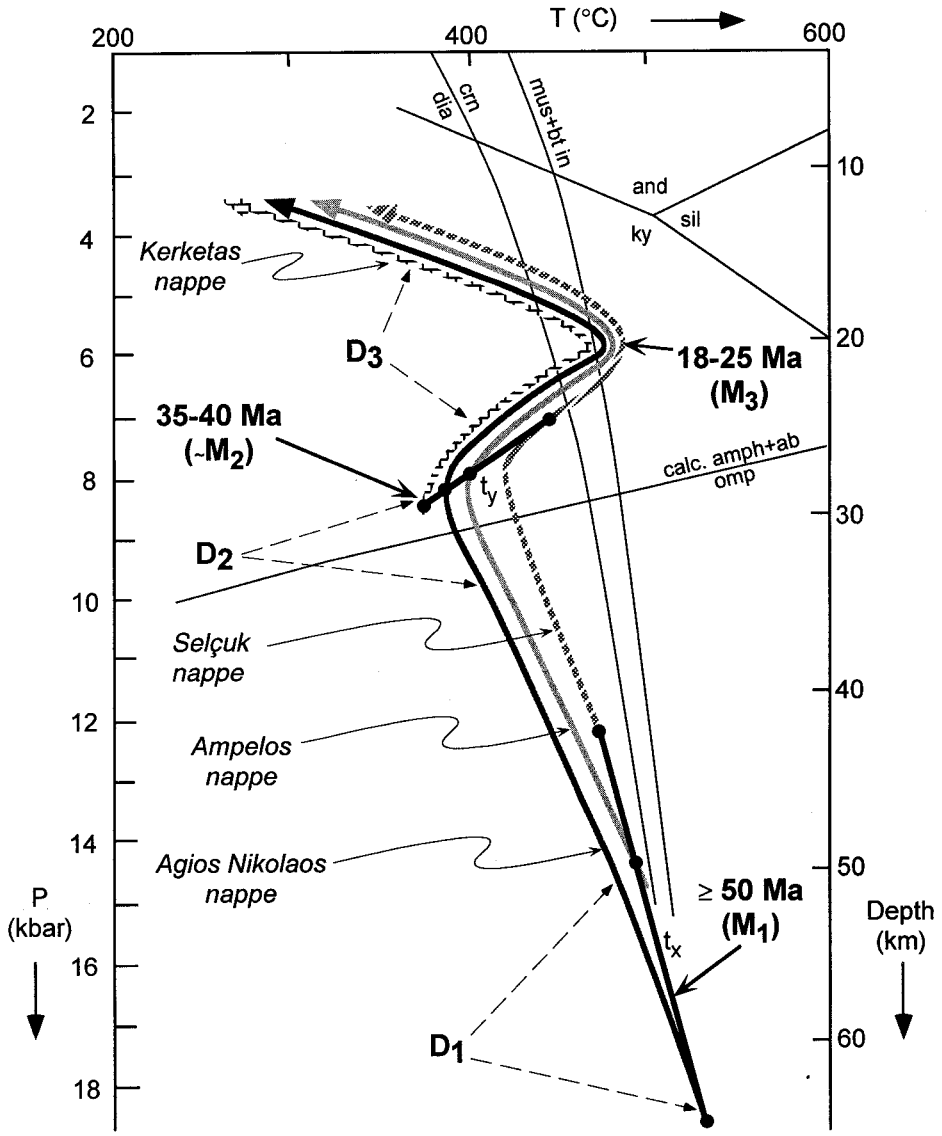

Fig. 6. Generalized *P–T* paths for the different metamorphic nappes in western Samos. Data from various sources as listed in Table 3; error bars have been omitted for clarity. The hypothetical time lines, t_x and t_y (thick solid lines) are meant to visualize that tectonometamorphic events affected the different nappes at different *P–T* conditions and that the stacking order of the four nappes is maintained during prograde M_3 metamorphism, i.e. that at a given time t_y the Kerketas nappe still represents the lowermost nappe in the sequence. Note that the Kallithea nappe (not shown) was emplaced late when the nappes of the Cycladic blueschist unit already reached the surface. Age constraints are from Altherr et al. (1982), Wijbrans and McDougall (1988), Wijbrans et al. (1990), Bröcker (1993) and Bröcker and Enders (1999). The barometric data are converted to depth assuming an average rock density of 2.8 g/cm^3.

kinematics of D_1 and D_2 exists. We first establish typical structural characteristics, deformation/metamorphism and overprinting relationships, and then illustrate key geologic aspects from the nappe contacts and the Pyrgos graben.

5.1. D_1/D_2 deformations

Deformation/metamorphism relationships indicate that the first two generations of ductile structures (D_1 and D_2) were related to blueschist- and transitional blueschist–greenschist-facies metamorphism (Fig. 7). In a few outcrops in the Agios Nikolaos and Ampelos nappes either overprinting relationships between D_1 and D_2 were observed or growth of blueschist-facies porphyroblasts occurred between D_1 and D_2 (Fig. 7a) which allowed us to distinguish between D_1 and D_2 structures. In most cases, however, both sets of structures are hard to distinguish and are therefore described together.

Much of the metapelite, quartzite, marble and metabasite of the Agios Nikolaos and Ampelos nappes and, in part, also the gabbro of the Selçuk nappe have a regionally shallow east-dipping S_1 foliation which is

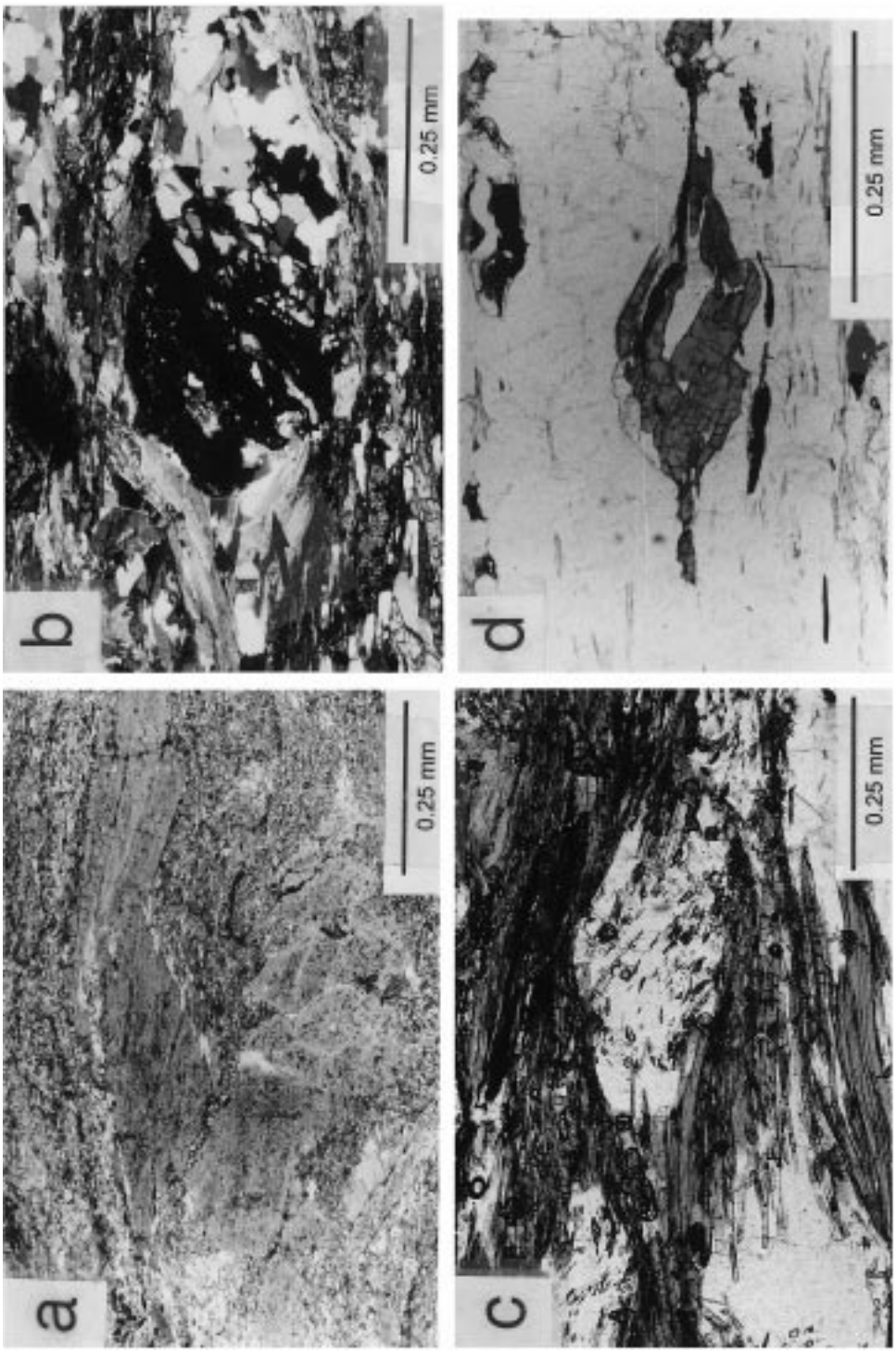

Fig. 7. Photomicrographs of $D_{1/2}$ structures in XZ sections ($X \geqslant Y \geqslant Z$ principal finite-strain axes). (a) Porphyroblastic glaucophane overgrowing S_1 statically. (b) Slightly rotated syn-D_1 garnet with strain shadow containing glaucophane (arrow). (c) Rotated D_2 albite prophyroblasts; calcic amphibole and sphene, both of which replace glaucophane, make up external and in part also internal foliation; sense of shear is top-to-the-SE. (d) Asymmetrically sheared chloritoid crystal in quarzite of Ampelos nappe directly above Pythagoras thrust; asymmetry indicates top-to-the-E sense of shear.

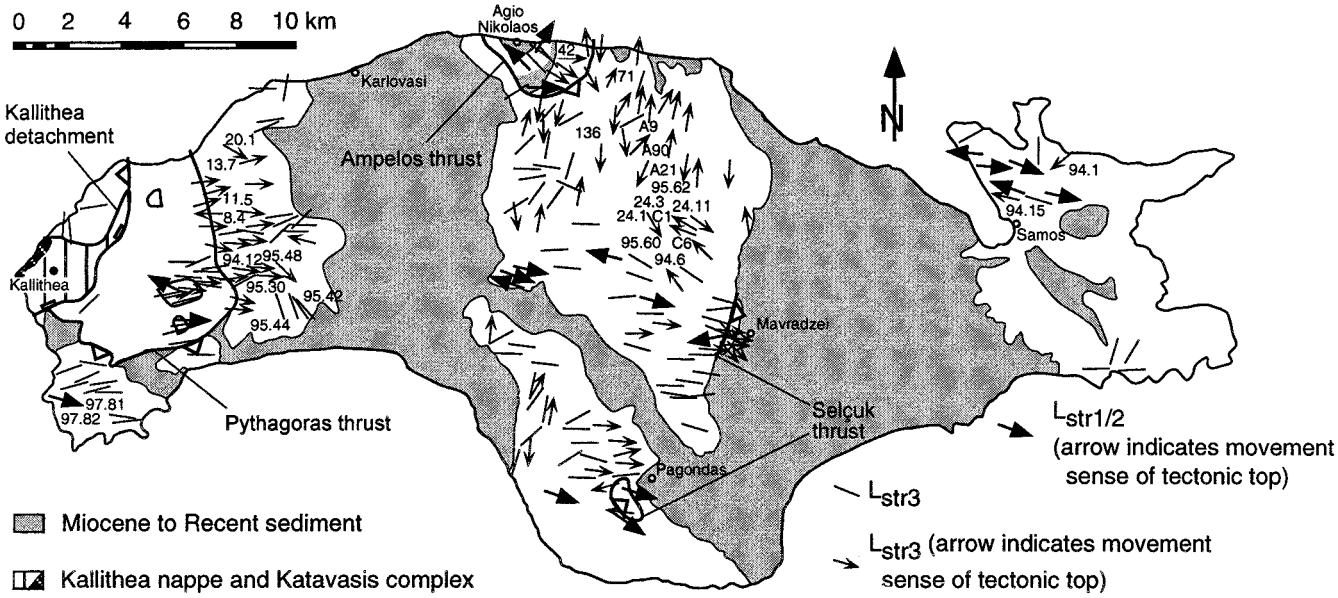

Fig. 8. Map of $L_{str1/2}$ and L_{str3} showing scarcity of $L_{str1/2}$ and variable orientation of L_{str3}. Each symbol represents mean of between 2 and 28 measurements in the vicinity of symbol. Localities of quartz-*c*-axis samples shown in Fig. 11 are indicated.

strongly transposed. S_1 is defined by glaucophane, phengite, paragonite, quartz, chlorite, epidote, albite, chloritoid, kyanite, zoisite, sphene and opaques. Omphacite and garnet also grew during D_1 (Fig. 7b). In a few cases it can be demonstrated in thin sections that S_1 is axial planar to rootless, highly sheared, small-scale folds (F_1). Static growth of glaucophane, chloritoid and kyanite followed S_1 and F_1.

D_2 structures are associated with the breakdown of glaucophane to barroisite, actinolite, white mica, albite and chlorite. Quartz veins folded during D_2 are commonly rootless with strongly attenuated limbs and thickened hinges. The quartz veins and S_1 were isoclinally folded about moderately ESE-plunging F_2 axes and in the hinges of F_2 folds a new S_2 foliation developed subparallel to S_1. In these zones, the orientation of S_1 is subparallel to the orientation of S_1 in zones where D_2 is weak or absent. Therefore, S_2 is regionally subparallel to S_1. Both foliations are commonly indistinguishable and then termed $S_{1/2}$. $S_{1/2}$ is commonly subparallel to the nappe contacts.

In some outcrops within the blueschist unit, glaucophane, barroisite, albite, white mica, chloritoid and kyanite are strongly lineated in $S_{1/2}$ and this lineation has a WNW–ESE orientation ($L_{str1/2}$, Fig. 5a). These mineral lineations are parallel to aligned quartz–albite aggregates and strain shadows around D_1 garnet and $D_{1/2}$ albite (Figs. 7b and c). R_f/ϕ analysis of quartz and albite grains in the quartz–albite aggregates shows that the maximum elongation direction of the quartz and albite grains parallels the alignment of the quartz–albite aggregates, suggesting that at least the quartz–albite alignment represents a true stretching lineation. In zones of strong $D_{1/2}$ deformation, R_f/ϕ work on dynamically recrystallized quartz grains yielded strain ratios of $X/Z \geqslant 4.5$ ($X \geqslant Y \geqslant Z$, principal strain axes). These are minimum estimates because quartz is recrystallized.

Kinematic indicators associated with $S_{1/2}$ are asymmetric strain shadows around garnet containing barroisite, chloritoid and glaucophane (Fig. 7b), rotated glaucophane, chloritoid and albite (Fig. 7c), asymmetries of chloritoid crystals (Fig. 7d), and asymmetries of $D_{1/2}$ isoclinal folds. The kinematic indicators do not supply a consistent sense of shear (Fig. 8).

The lack of a consistent sense of shear might be due to a general non-coaxial deformation. To verify this, the degree of non-coaxiality for $D_{1/2}$ was estimated using the approach of Wallis et al. (1993). In a general shear-flow regime, particles with an aspect ratio above a critical value will rotate until they reach a stable orientation whereas particles below this critical value will rotate freely (Jeffery, 1922; Ghosh and Ramberg, 1976). According to Passchier (1987), the value of this critical aspect ratio (R_C) is a function of the degree of non-coaxiality (W_m) only, and is expressed by:

$$W_m = R_C^2 - 1/R_C^2 + 1.$$

Critical prerequisites for applying this method are reasonably homogeneous deformation at the mesoscopic scale and a relatively large number of particles (Passchier, 1987). Five samples of chloritoid–kyanite schist from the Ampelos nappe containing abundant syn-D_1 chloritoid porphyroblasts and another three samples of Ampelos metabasite containing abundant

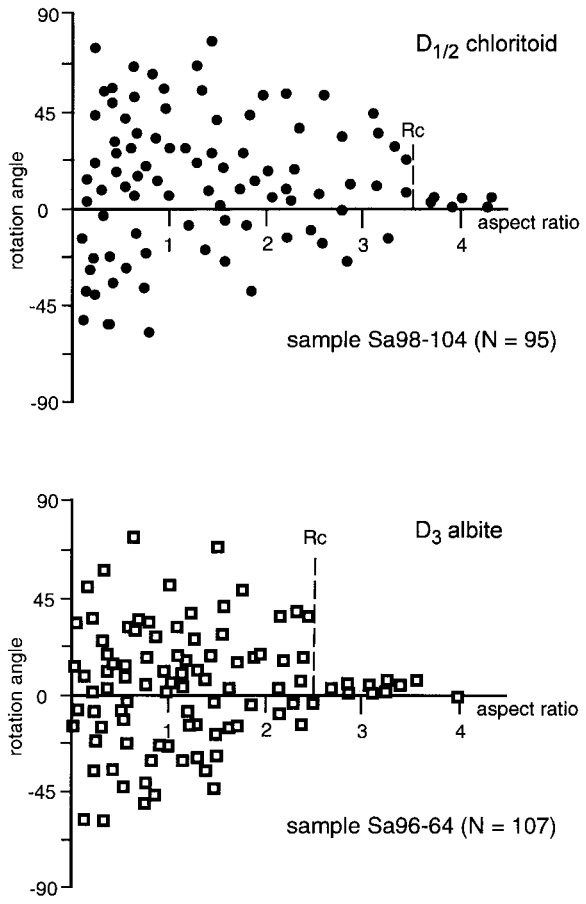

Fig. 9. (a) Aspect ratio plotted against rotation angle of chloritoid porphyroblasts in chloritoid–kyanite schist. The rotation angle is the angle between the long axis of chloritoid and the $S_{1/2}$ foliation. The dashed line defines the critical aspect ratio (R_C) which divides objects whose long axes reached a stable position subparallel to the foliation and those with lower aspect ratios that did not find a stable position and thus show a large scatter in readings. R_C is interpreted to be close to 3.5 which corresponds to a value of $W_m = 0.85$. (b) Plot for syn-D_3 albite porphyroblasts in chlorite–albite schist. R_C is interpreted to be close to 2.5 which corresponds to a value of $W_m = 0.72$.

syn-D_2 albite were selected, and the rotation angles of the porphyroblasts were measured with respect to the mesoscopic $S_{1/2}$ foliation. The results for one representative sample is shown in Fig. 9(a). The values for R_C range from 2.9 to 3.6; the mean of R_C for the five samples containing D_1 chloritoid crystals is 3.3 (corresponding to $W_m = 0.83$), and the mean of the three samples containing D_2 albite is $R_C = 3.2$ which corresponds to $W_m = 0.82$.

5.2. Main D_3 deformation

D_3 structures were associated with greenschist-facies mineral assemblages. In some outcrops, we observed that $S_{1/2}$ has been thrown into a set of isoclinal, commonly rootless F_3 folds. F_3 folds have similar morphological characteristics to $F_{1/2}$ folds. The S_3 foliation is defined by oriented growth of chlorite, albite, quartz, white mica and, in part, biotite and actinolite or a differentiated layering of quartz and sheet silicates on a 0.3–1.5 mm scale. S_3 transposed $S_{1/2}$ and became the dominant regional foliation (Fig. 5b). An associated stretching lineation (L_{str3}) characterized by the preferred orientation of mica and chlorite, aligned quartz aggregates and quartz fibres in strain shadows developed. R_f/ϕ analysis of quartz grains in the quartz aggregates and in phyllosilicate-bearing quarzite shows that the maximum elongation direction of the quartz grains parallels the alignment of the quartz aggregates and the preferred orientation of mica and chlorite. L_{str3} has a variable orientation across the island (Figs. 5c and 8). In addition to L_{str3}, a crenulation lineation (L_{cren3} in Fig. 5d), is defined by the intersection of $S_{1/2}$ and S_3. Throughout the region of strong D_3 shear, where D_3 tectonites are mylonitic and R_f/ϕ work on dynamically recrystallized quartz grains yielded strain ratios of $X/Z \geqslant 5$, the angle between L_{str3} and L_{cren3} and F_3 axes does not exceed 10°. In intervening low-strain areas, the angle between L_{str3} and L_{cren3} and F_3 is of the order of 45–60° (in low-strain areas, strain ratios as obtained from R_f/ϕ analysis of dynamically recrystallized quartz were $X/Z \leqslant 3$).

A detailed description of consistent top-to-the-E/ENE D_3 sense-of-shear indicators directly above the Selçuk and Pythagoras thrusts (see also Fig. 10a) will be given below. Away from these nappe contacts, especially in the central part of the island, the shear senses are less consistent (Figs. 8 and 11), although we infer a general top-to-the-E/ENE sense of shear from the data.

Microstructures show that Fe–Mg silicates were substantially altered to chlorite during D_3 (Fig. 10b). In zones of strong D_3 deformation, glaucophane-bearing metabasite has been completely reconstituted to chlorite–albite schist. Most of the albite grew during D_3 as indicated by rotated D_3 microstructures within albite. Garnet also grew during the early stages of D_3. Microprobe work on phengite and chlorite in D_3 strain shadows shows that D_3 structures started to develop at different stages. Early D_3 structures are frequent in the Agios Nikolaos nappe and the lower parts of the Ampelos nappe and developed before the climax of M_3, i.e. before the growth of biotite and M_3 garnet. Phengite barometry (Massone, 1995) suggests that the early D_3 structures started to develop at about 7 kbar with phengites in the Agios Nikolaos nappe having slightly but consistently higher Si values per formula unit than those in the Ampelos nappe.

However, in most of the Ampelos nappe, especially in its upper parts, but also in the other nappes of the Cycladic blueschist unit, D_3 structures developed during and closely after the peak of M_3 metamorphism. These late D_3 structures are more frequent than

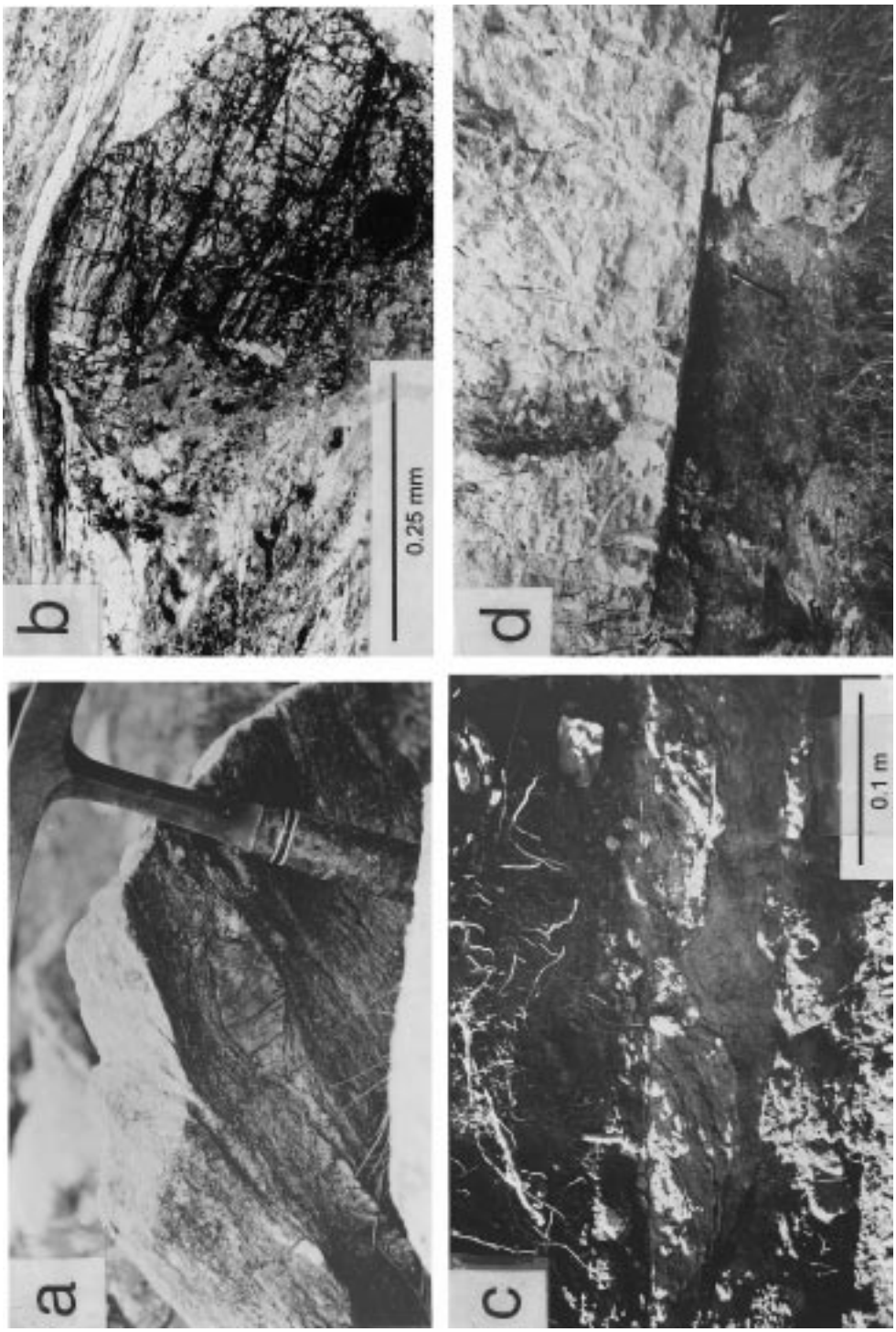

Fig. 10. Photomicrographs of D_3 structures. (a) Rotated marble clast in calcareous phyllite above the Pythagoras thrust on the eastern side of the Kerketas Massif indicating top-to-the-E sense of shear. (b) Asymmetric strain shadow around garnet; note that garnet breaks down to chlorite; sense of shear is top-to-the-E. (c) Riedel structures at the base of the Kallithea nappe; sense of shear is top-to-the-NW. (d) Outcrop photograph of cataclastic fault zone at the top of the Katavasis complex north of Kallithea where Kerketas nappe (upper half of photograph) occurs between Katavasis complex and Kallithea nappe.

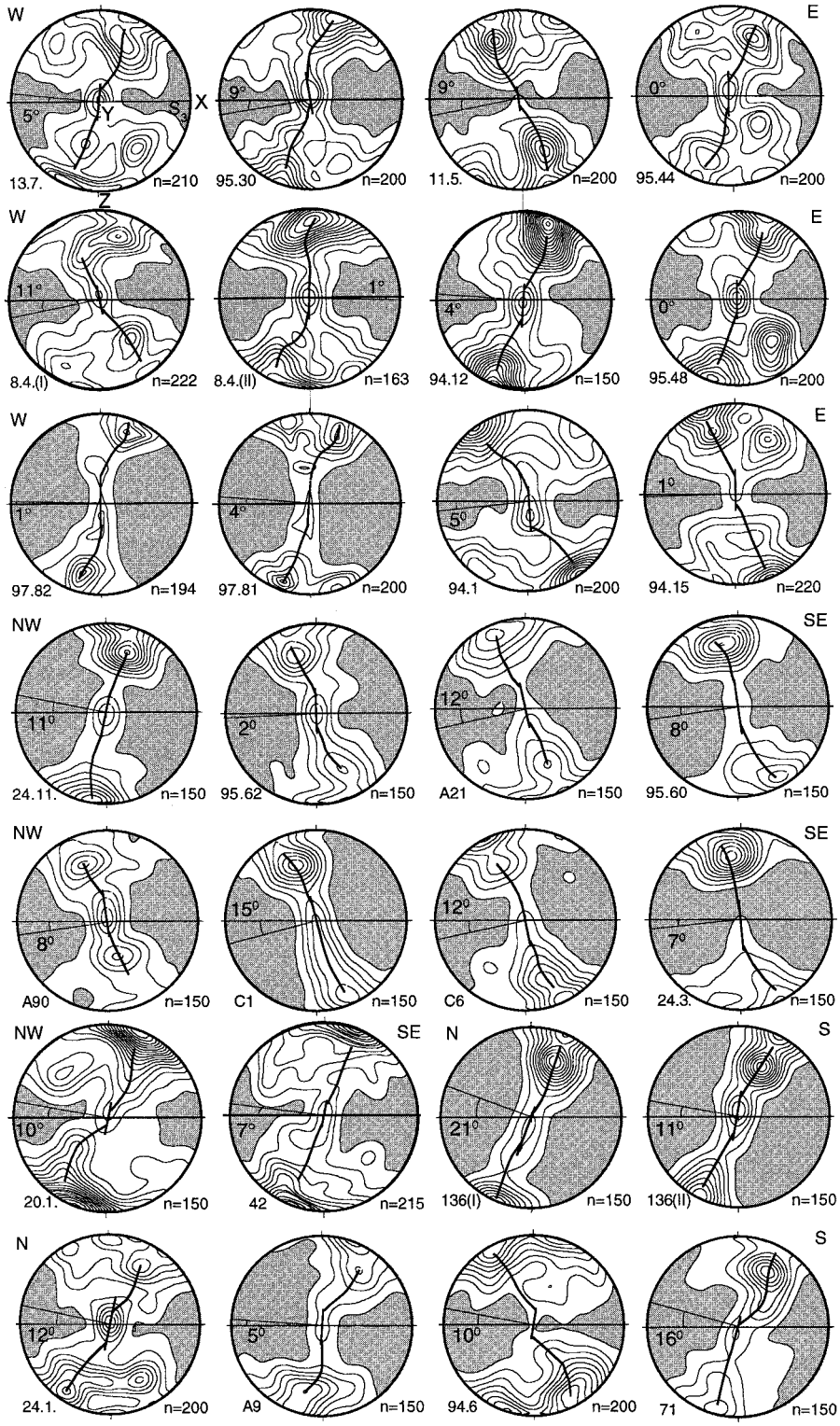

Fig. 11. Quartz *c*-axis fabrics from D_3 tectonites from various parts of Samos Island (for localities of samples refer to Fig. 8); principal strain axes *X*, *Y* and *Z* and the S_3 foliation have the same position for all samples and are only indicated for sample 13.7 (upper left-hand side). The angle β between the central part of the fabric skeleton and the S_3 foliation, the sample numbers and the number of measured grains is also shown. Most of the fabrics have a kinked or roughly orthorhombic topology suggesting deformation with $0<W_m<1$. The fabrics do not have a consistent sense of asymmetry although we interpret the majority of the fabrics to indicate a top-to-the-E sense of shear.

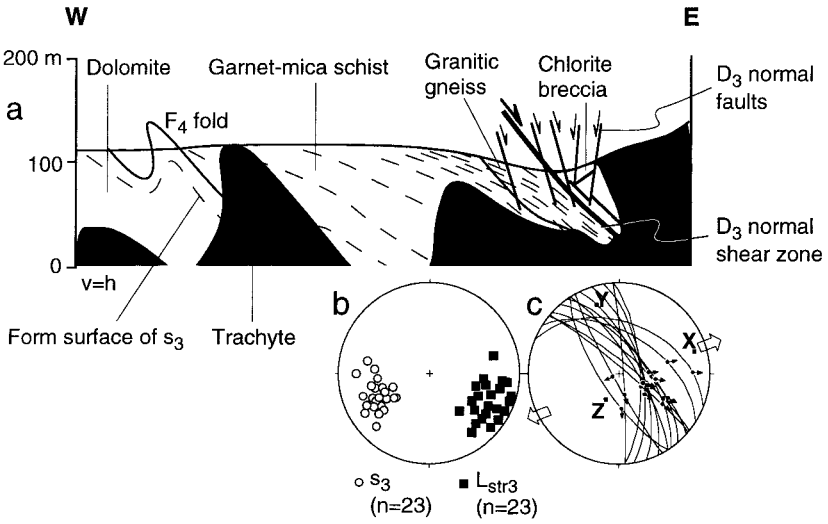

Fig. 12. (a) E–W cross-section through Agios Nikolaos nappe showing prominent late D_3 shear zone and D_3 faults. (b) Stereographic projection of S_3 and L_{str3} from this late D_3 shear zone. (c) Fault-slip data from D_3 faults that occur above and partly cut across late D_3 shear zone. The orientation of each fault is illustrated by great circles; the arrows indicate the relative sense of slip as deduced from slickenside measurements on the fault planes; principal strain axes are shown; the large open arrows indicate the deduced extension direction.

early D_3 structures and are characterized by asymmetric strain shadows around M_3 garnet (Fig. 10b). Biotite in these strain shadows was almost completely replaced by chlorite. Some of the late-D_3 ductile structures progressively grade structurally upwards into D_3 normal faults (Fig. 12).

In order to quantify the degree of non-coaxiality for the D_3 deformation, six samples of chlorite–albite schist from within the Ampelos nappe containing abundant syn-D_3 albite porphyroblasts were selected, and the rotation angles of the porphyroblasts were measured with respect to the mesoscopic S_3 foliation. The result for one of the samples is shown in Fig. 9(b). The values for R_C range from 1.9 to 2.4; the mean of R_C for the six samples is 2.2 which is equivalent to $W_m = 0.71$.

5.3. D_4 and D_5 deformations

Ductile deformation in the Cycladic blueschist unit during D_4 was very limited and not accompanied by extensive recrystallization and grain growth. Fabrics associated with D_4 are therefore not pervasively developed. The most prominent D_4 structures are folds at the 10–>100 m scale that have been observed in the blueschist unit and in the cover. S_3 has been thrown into a set of mostly tight, commonly west-vergent F_4 folds. F_4 folds in the deeper parts of the blueschist unit are tight and associated with a generally NE-dipping crenulation cleavage (S_4, Fig. 5e). Here, the older S_3 foliation is crenulated and in part kinked, and irregular or stylolitic solution-transfer seams marked by concentrations of opaques, sericite and chlorite form a spaced S_4 cleavage. The seams wrap around and thus postdate M_3 albite and garnet porphyroblasts. The intersection of S_4 with S_3 created a pronounced intersection lineation (L_{cren4}) that defines a strong NNE-trending maximum (Fig. 5f). Higher in the sequence, F_4 folds are open to tight with E-dipping to subvertical axial planes and NW/N-trending axes (Fig. 5f). Other prominent D_4 structures are discrete reverse faults, the planes of which dip mainly to the east, but also to the west (Figs. 13–16). A prominent WSW-dipping D_4 reverse fault is exposed at the contact between the Ampelos nappe and the Mytilini graben at the north coast (Boronkay and Doutsos, 1994) and places marble onto Early Tortonian marls of the Hora Formation. D_4 structures only occur in Miocene sediments below the unconformity at the base of the Mytilini Formation, supplying an age constraint for D_4.

D_5 is an entirely brittle event and includes a set of E–W- to NW-striking faults which have a normal sense of displacement. The map pattern (Fig. 2) demonstrates that D_5 faults crosscut all other structures and occur in all exposed rock units in Samos. The map furthermore shows that early D_5 faults have curved outcrop traces and are cut by steeper normal faults that have relatively straight outcrop patterns. NW-striking D_5 faults appear to be the latest set of D_5 faults. Both sets of D_5 normal faults are due to N/NE-oriented extension (Figs. 4, 15 and 16).

5.4. Ampelos thrust

The Ampelos thrust separates the Ampelos and Agios Nikolaos nappes. The Ampelos thrust was severely affected by later deformations and is poorly

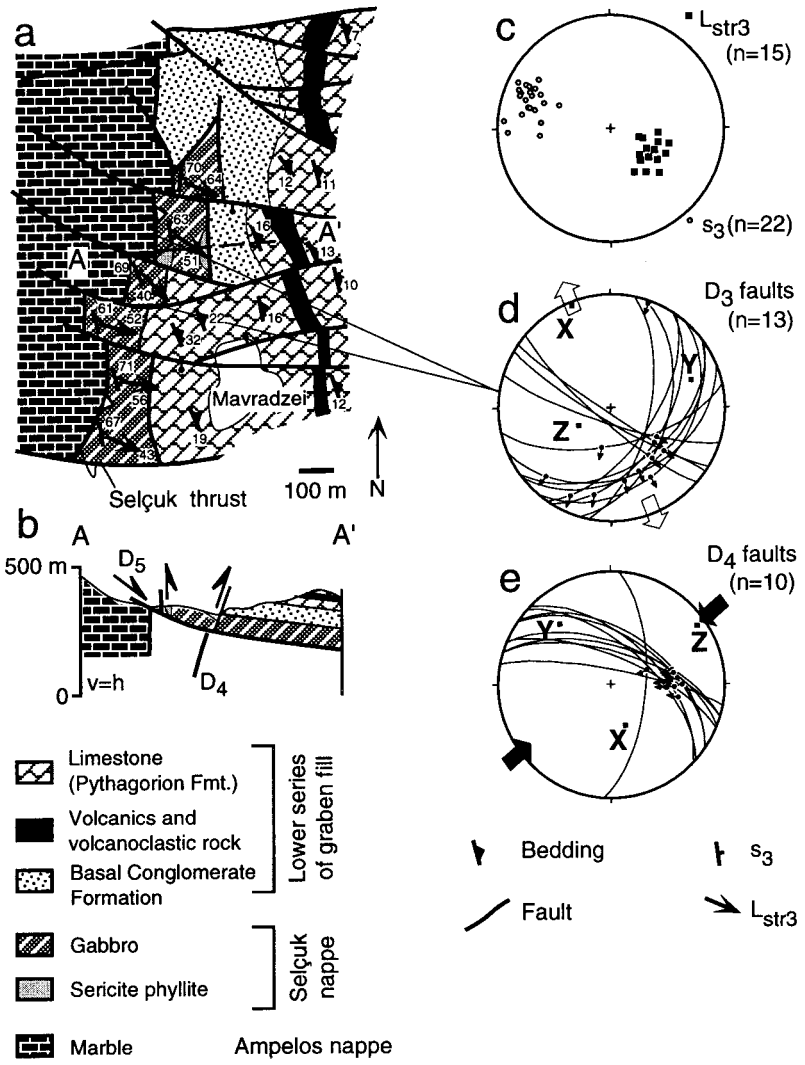

Fig. 13. (a) and (b) Detailed map and cross-section of Selçuk thrust west of Mavradzei (see Fig. 2 for map location). (c) Stereographic projection of S_3 and L_{str3}. (d) and (e) Fault-slip data from D_3 and D_4 faults; open arrows indicate extension direction and filled arrows show contraction direction.

exposed. Garnet-mica schist directly underneath the Ampelos thrust north of Agios Nikolaos preserved D_1 structures. D_1 shear-sense indicators are internal foliations within rotated M_1 garnet and asymmetric strain shadows around M_1 garnet which contain glaucophane (Fig. 7b). The rocks of the Ampelos nappe above the Ampelos thrust were strongly sheared during D_3 and therefore D_1 fabrics are rare. In general, D_1 kinematic indicators do not supply a consistent sense of shear in the Agios Nikolaos area.

Within the Agios Nikolaos nappe a discrete, late D_3 shear zone is exposed (Fig. 12a). The granitic gneiss depicts a moderately to steeply E-dipping mylonitic S_3 foliation. On S_3 an ESE-plunging L_{str3} (Fig. 12b) associated with top-ESE shear-sense indicators developed. The mylonitic foliation is characterized by chlorite and quartz ribbons and grades structurally upwards into a cataclastic foliation in which feldspar and quartz are intensely fractured. The fractures are commonly associated with red–brown iron oxides. Fracturing is accompanied by growth of chlorite, in part as fibrous overgrowth. The ductile and brittle–ductile structures are cut by faults whose kinematics is similar to that of the ductile structures (Fig. 12). The granitic gneiss is interlayered with mica schist that grades over a short distance into a chlorite breccia. The chlorite breccia is cut by moderately dipping faults which are in turn cut by steeply dipping faults. The latter two sets of faults dip either to the SE or NW, and their kinematics is again similar to the ductile fabrics in the granitic gneiss (Fig. 12).

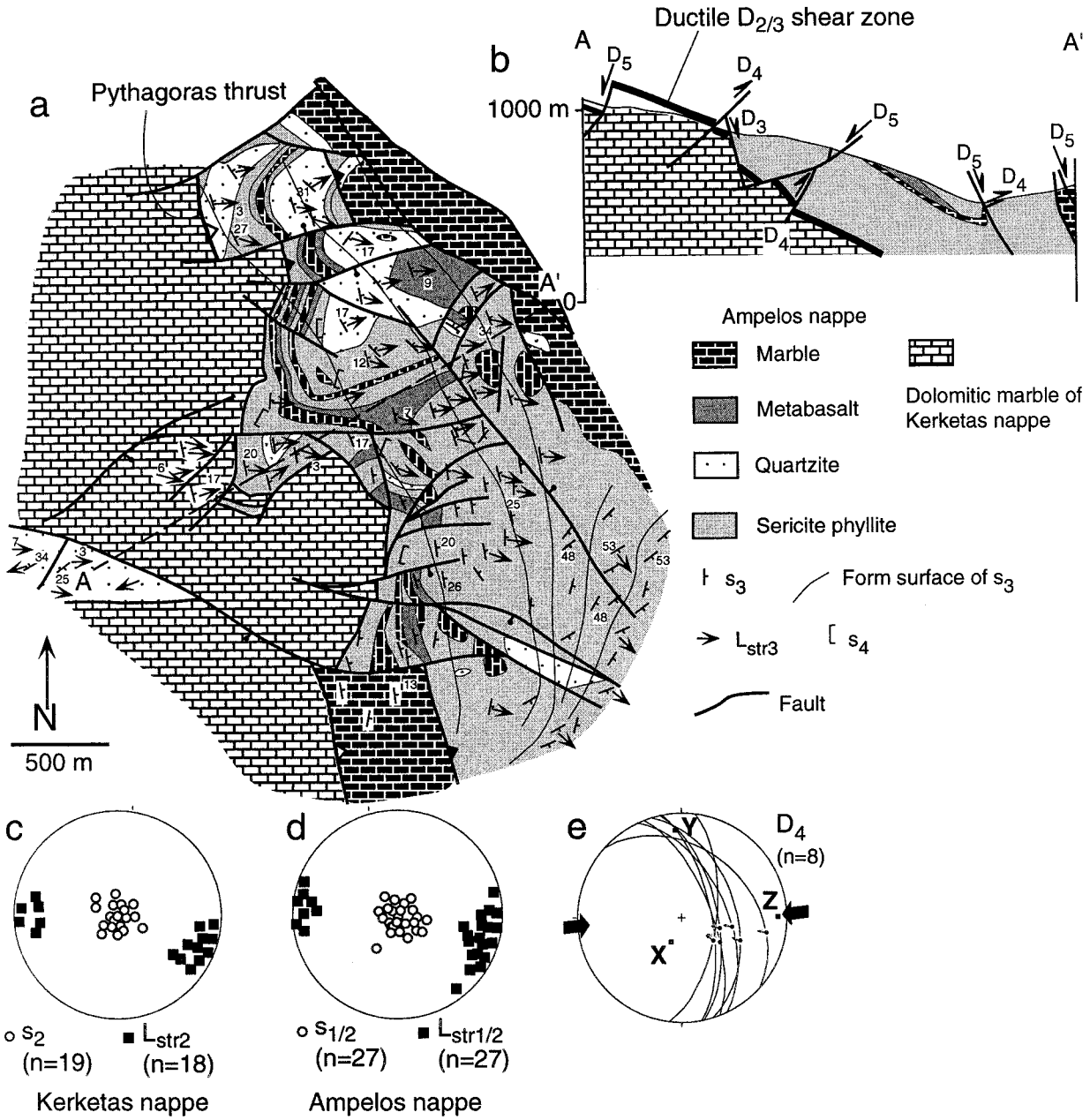

Fig. 14. (a) and (b) Detailed map and cross-section of Pythagoras thrust at the eastern side of the Kerketas Massif (refer to Fig. 2 for location of map). The ductile D_2/D_3 shear zone in the cross-section is shown schematically. Attenuation of section above the Kerketas nappe is documented by omission of the Agios Nikolaos nappe and direct contact of marble of the Ampelos nappe with dolomitic marble of the Kerketas nappe. (c) and (d) Stereographic projection of pre-D_3 foliations and stretching lineations from (c) Kerketas and (d) Ampelos nappes. (e) Fault-slip data and principal strain axes of D_4 faults.

5.5. Selçuk thrust

The Selçuk thrust is best exposed west of the village of Mavradzei (Fig. 13). Here, the Selçuk nappe is represented by strongly sheared flaser gabbro, which contains relic magmatic diopside. The diopside is marginally replaced by rare glaucophane, which in turn is severely transformed into blue–green calcic amphibole. The latter defines, together with albite, clinozoisite, epidote and quartz, an S_2 foliation. Associated kinematic indicators are characterized by the replacement of glaucophane to barroisite and supply a top-to-the-W sense of shear. However, in a less well exposed part of the Selçuk thrust southwest of Pagondas, rare kinematic indicators supply a top-to-the-E sense of shear.

The relic S_2 foliation is overprinted by a mylonitic ESE-dipping S_3 foliation (Fig. 13c). In rare cases, the

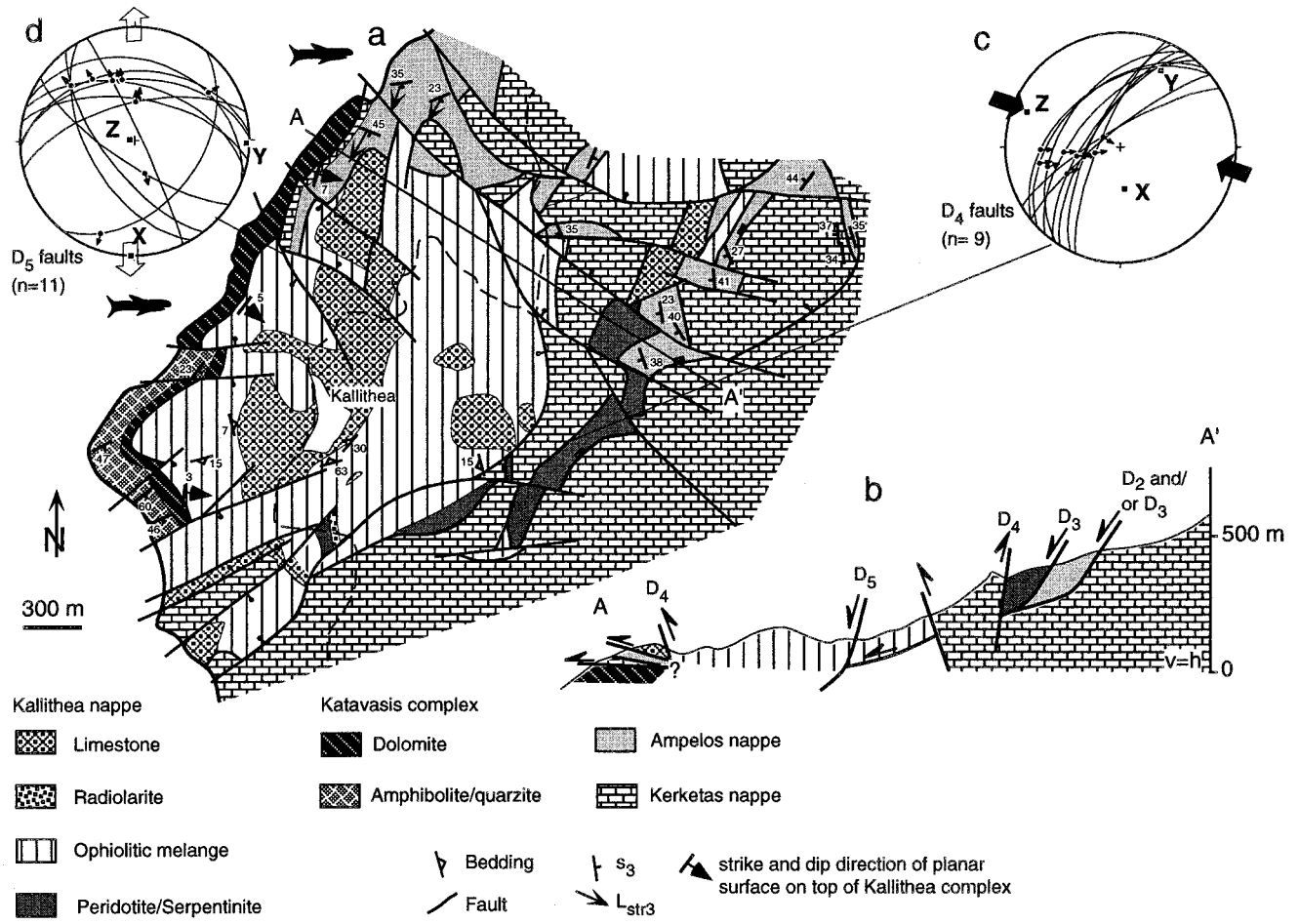

Fig. 15. (a) and (b) Detailed map and cross-section of Kallithea nappe and adjacent units (see Fig. 2 for location). The contact between the Katavasis complex and the Kallithea and Kerketas nappes, respectively, is marked by a conspicuous ~50 cm thick dark-grey cataclasite (Fig. 10d). Scarcity of overprinting relationships does not allow a decisive interpretation of the relationship between the Kallithea nappe and the Katavasis complex. (c) and (d) Fault-slip data from D_4 and D_5 faults.

new S_3 foliation cuts S_2 at a higher angle and is characterized by the replacement of barroisite by actinolite. The S_3 foliation contains a down-dip stretching lineation (L_{str3}) defined by elongated quartz and actinolite aggregates. Associated kinematic indicators are asymmetric strain shadows around amphibole porphyroblasts, which supply a top-to-the-ESE sense of shear.

Commonly, the steeply dipping foliation planes contain shiny, striated surfaces. The first set of brittle structures produced moderately SE-dipping striations that occur on reactivated S_3 planes and on newly formed outcrop-scale faults (Fig. 13d). Riedel planes of up to one metre in size indicate a dextral, down-dip sense of shear. In thin section, a weak P foliation (sensu Rutter et al., 1986) defined by solution-transfer seams and chlorite can be observed within the composite Riedel structures.

A younger set of crosscutting, subvertical striations also occurs on S_3 planes and on small-scale faults that cut across D_3 faults. Small-scale Riedel structures yielded a reverse sense of shear due to E–W contraction (D_4) (Fig. 13e). D_4 faults are cut by E–W-trending D_5 normal faults (Fig. 13a).

5.6. Pythagoras thrust

The Pythagoras thrust separates the Kerketas nappe from the Ampelos nappe. Impure dolomitic marble of the Kerketas nappe immediately below the Pythagoras thrust at the eastern side of the Kerketas Massif in part preserved D_2 structures. These are a foliation made up by phengite, chlorite, talc, quartz, calcite and opaques and a WNW-trending stretching lineation expressed by phengite alignment. The penetrative foliation and chloritoid alignment in Ampelos quarzite immediately above the Pythagoras thrust has the same orientation (Fig. 14). R_f/ϕ analysis of quartz grains in the quartzite shows that the maximum elongation direction of the quartz grains parallels the phengite and chloritoid alignment, suggesting that this lineation is a true stretching lineation. The chloritoid preserved

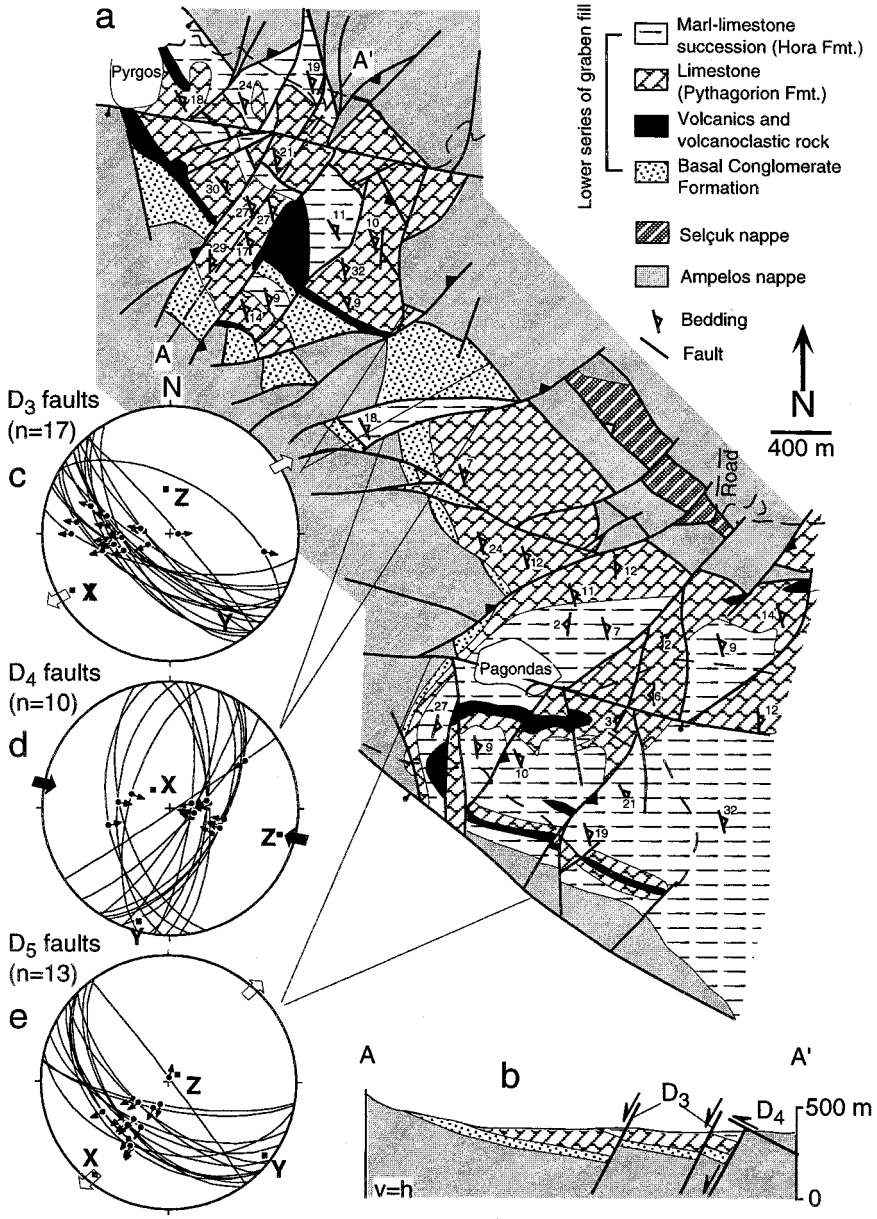

Fig. 16. (a) and (b) Detailed map and cross-section of Pyrgos graben (see Fig. 2 for location); note general half-graben architecture. (c), (d) and (e) Fault-slip data from D_3, D_4 and D_5 faults.

asymmetric internal fabrics suggesting a top-to-the-E sense of shear during D_2 (Fig. 7d).

Penetrative ductile D_3 structures in the Ampelos nappe above the Pythagoras thrust are an E-dipping S_3 and an E-plunging L_{str3}. L_{str3} immediately above the nappe contact is associated with abundant and consistent top-to-the-E kinematic indicators (Figs. 8, 10a and 11).

The D_3 structures are in turn strongly overprinted by D_4 faults. Faulting caused pronounced cataclasis of the Kerketas dolomite, which resulted in a structureless, fine-grained microstructure in the dolomite adjacent to the fault. Fault-slip analysis indicates that faulting is due to E–W contraction (Fig. 14c). D_4 reverse faults are then cut by W/NW-trending D_5 normal faults.

5.7. Kallithea detachment

A structural analysis in the Kallithea nappe is hampered by severe and in part chaotic brittle disruption of all lithological units and poor outcrop conditions. The partly serpentinized peridotite and the ophiolitic mélange at the base of the Kallithea nappe are cataclastically sheared resulting in a crude, spaced P foliation. The P foliation is defined by the preferred orientation of tabular fragments or compositional layering in clayey and serpentinitic matrix and inclined

planar, subparallel, continuous faults that bound the shear zones. This basal cataclastic shear zone, which we refer to as the Kallithea detachment (Fig. 8), may contain radiolarite fragments embedded in a dark matrix composed of clayey material and disrupted mafic rock. Rare kinematic indicators include Riedel planes that are inclined with respect to the shear-zone-bounding faults in a sense opposite to that of the P foliation, and asymmetric small-scale folds. These shear-sense indicators imply a top-to-the-NW/NNW offset (Fig. 10c).

The contact between the Kallithea nappe and the Katavasis complex is characterized in the field by a distinct, knife-sharp, planar, <50-cm-thick layer of severely cataclastically reworked dolomite at the top of the Katavasis complex (Figs. 10d and 15). Dolomite porphyroclasts are intensely fractured. Alteration during cataclasis was associated with pronounced influx of fluids, which caused the development of phyllosilicate and clay minerals and produced the dark-grey matrix. Kinematic indicators are Riedel planes and P foliations that yielded a top-to-the-WNW/NNW sense of shear. Below this thin cataclastic zone, the dolomite has not been affected by cataclasis at all.

Our mapping indicates that the Kallithea detachment is cut by D_4 and D_5 faults (Fig. 15) suggesting that it is a D_3 structure. The shear zone on top of the Katavasis complex is cut by D_5 normal faults; however, no overprinting relationships between rare D_4 faults in this area and the cataclastic shear zone have been observed. Nevertheless, the 10 Ma dikes in the Katavasis complex (Table 1) never cut through the knife-sharp fault on top of the Katavasis complex, suggesting that movement along this fault is younger than 10 Ma.

5.8. Pyrgos graben

The tectonic significance of the Middle Miocene graben in the Aegean Sea is controversial. The graben were either assumed to be Miocene extensional basins (Le Pichon and Angelier, 1979) or were interpreted as transpressional features (Boronkay and Doutsos, 1994). In the Karlovasi and Mytilini graben, the sediments either onlap the metamorphic rocks or the contact between the sediments and the metamorphic rocks is highly overprinted by brittle faulting that postdated graben formation. Nevertheless, structural relationships in the Pyrgos graben (Fig. 16) allow us to shed some light on graben formation.

Our mapping established a pattern of faults, which have regionally coherent overprinting relationships with each other. The earliest faults in the Pyrgos graben are WNW/NW-striking D_3 faults. These faults are in turn cut by a set of N/NE-striking D_4 faults. The youngest set of structures (D_5) are approximately WNW-striking faults. The cross-section (Fig. 16b) reveals a half-graben geometry of the Pyrgos graben with a major graben-bounding fault at the northeastern side and onlapping geometries at the southwestern side of the graben. Fault-slip analysis reveals that D_3 resulted from ENE/NE horizontal extension followed by WNW-oriented horizontal contraction during D_4, which in turn is succeeded by NE horizontal extension during D_5 (Fig. 16c–e). Crosscutting striations on D_3 faults show that during D_4 and D_5 some D_3 faults were reactivated.

6. Tectonic interpretation

6.1. D_1 and D_2 crustal contraction

Although the kinematic data for D_1 and D_2 do not supply a consistent sense of shear, they do suggest WSW–ESE tectonic transport. These structures probably formed in the Eocene and earliest Oligocene (Fig. 6) and therefore predated the Miocene $\sim 30^\circ$ anticlockwise rotation described by Kissel and Laj (1988). If the effects of this rotation were removed, the data for D_1 and D_2 would indicate NW–SE tectonic transport during and shortly after high-pressure metamorphism.

Kinematic indicators for the early orogenic evolution in the Aegean are scarce. Vandenberg and Lister (1996) reported NW-trending glaucophane lineations from Ios Island. The only shear-sense data for deformation associated with blueschist-facies metamorphism we are aware of are those of Ridley (1984) from Syros Island which indicate top-to-the-SE tectonic transport. Eocene to earliest Oligocene top-to-the-SE tectonic transport towards the foreland is in accord with Late Cretaceous to Eocene top-to-the-SE tectonic transport of the overlying Lycian nappes (Collins and Robertson, 1998), general southward progradation of orogenesis in the Aegean and top-to-the-S tectonic transport during Early Miocene high-pressure metamorphism in Crete (e.g. Fassoulas et al., 1994).

We have not been able to relate the mesoscopic D_1 and D_2 structures unequivocally to nappe contacts. Deformation/metamorphism relationships (Fig. 6) indicate that the nappe pile of the Kerketas, Agios Nikolaos, Ampelos and Selçuk nappes was largely assembled prior to D_3/M_3 and therefore formed during D_1 and D_2. The P–T estimates show that the degree of M_1 metamorphism within the Cycladic blueschist unit decreases from the Agios Nikolaos nappe upward towards the Selçuk nappe. Therefore, and because D_1 and M_1 were followed by a stage of porphyroblastic glaucophane growth, we suggest that initial stacking of the Agios Nikoloas, Ampelos and Selçuk nappes took place during underthrusting and underplating

that caused deep burial and maximum metamorphic pressure.

During D_2 the Cycaldic blueschist unit was emplaced onto the Kerketas nappe along the Pythagoras (out-of-sequence) thrust. Deformation/metamorphism relationships show that D_2 structures formed during decompression indicating considerable exhumation of the Cycladic blueschist unit during D_2 (Fig. 6, see Avigad et al., 1997 for a similar case from Evia Island). These constraints also demand that the Pythagoras thrust must have moved upward relative to the Eocene/Oligocene Earth's surface in the direction of tectonic transport and therefore resulted from horizontal crustal contraction (cf. Wheeler and Butler, 1994). Thrusting of the Cycladic blueschist unit onto a cold foreland unit, i.e. the Kerketas nappe, caused cooling of the blueschists (Fig. 6). Lister and Raouzaios (1996) described a similar case of nappe stacking during initial decompression and rapid cooling of the Cycladic blueschist unit from the island of Sifnos.

The pressure drop during D_2 thrusting requires the removal of ~30–40 km of overburden above the Agios Nikolaos nappe. There is no evidence for Eocene to earliest Oligocene normal faults in the Aegean. The Lycian nappes, which overly the Cycladic blueschist unit in western Turkey show no evidence for normal faulting during this period of time (Collins and Robertson, 1998). Using a value of $W_m = 0.83$ and $R_{X/Z} \geqslant 4.5$ yields a vertical shortening of more than 30% in zones of strong $D_{1/2}$ deformation (note that this is a minimum estimate because recrystallized quartz grains were used for strain quantification). Ring (1998) showed that a value of $>30\%$ vertical shortening in the hanging wall of the Pythagoras thrust associated with an erosion rate <1 mm/a is sufficient to account for the removal of ~30–40 km of metamorphic section within and above the Cycladic blueschist unit. (Note that in order to properly estimate the contribution that $>30\%$ vertical shortening of the Cycladic blueschist unit made to the total exhumation of this unit, both the vertical rate at which the blueschist moved upwards through the overburden and the rate of thinning of the remaining overburden at each step along the exhumation path has to be considered, i.e. the velocity-gradient field along the exhumation path has to be specified for both the blueschist and its cover (Feehan and Brandon, 1999; Ring and Brandon, 1999)).

6.2. D_3 crustal extension

The overall geometric relationship between D_3 structures which overprinted the E-dipping Pythagoras and Selçuk thrusts, the consistent D_3 top-to-the-E kinematic indicators immediately above both thrust planes and the general attitude of bedding in the graben sediments in the vicinity of the thrusts (which provides a relation between the fault plane and the Earth's surface in the Miocene), suggests that top-to-the-E shear during D_3 descended relative to the Earth's surface in the direction of tectonic transport and therefore was caused by horizontal crustal extension. Crustal extension during D_3 is corroborated by the progressive development from ductile to brittle conditions of D_3 structures in the footwall of the D_3 shear zone south of Agios Nikolaos. There, the parallelism between mylonitic L_{str3} and the extension direction as deduced from fault-slip analysis suggests kinematic compatibility during progressive D_3 exhumation. The continuous evolution of these D_3 structures from ductile to brittle conditions resembles the structural evolution in the footwall of extensional faults in the Basin-and-Range province and other well-known extensional settings (e.g. Lister and Davis, 1989). Likewise, the identical kinematics of ductile D_3 structures and their brittle overprint at the Selçuk thrust west of Mavradzei implies kinematic compatibility during progressive exhumation. The D_3 half-graben geometry in the Pyrgos graben supplies further evidence for crustal extension during D_3.

Despite the consistent D_3 kinematic indicators at the Pythagoras and Selçuk thrusts, D_3 structures within the Ampelos nappe are somewhat difficult to interpret. The overall lack of a strong preferred orientation of L_{str3} across the island and the variable sense of shear may suggest a relatively strong component of coaxial flattening during D_3. W_m of about 0.71 proves pronounced deviations from simple-shear deformation and together with $R_{X/Z} \geqslant 5$ gives a minimum vertical shortening of more than 50% in zones of strong D_3 shear. We suggest that D_3 crustal extension was characterized by pronounced vertical shortening in a complexly ductilely flowing crust. Shear strains apparently localized heterogeneously around pre-existing structures and contacts in the extending rock mass (cf. Vandenberg and Lister, 1996).

The scarcity of overprinting relationships in the Kallithea region hinders an exact interpretation of the relationship between the Kallithea nappe and the Katavasis complex. Two general scenarios are discussed. (1) In the cross-section in Fig. 17(a), the D_3 extensional Kallithea detachment is cut by a knife-sharp D_4 thrust that eventually brought the Kallithea nappe on top of the Katavasis complex. In this interpretation, the Katavasis complex and the Kallithea nappe would have occupied very different paleogeographic positions—the Kallithea nappe originated in an internal position, whereas the occurrence of the Katavasis complex even below the Kerketas nappe indicates an external origin. This palinspastic inference is not corroborated by the regional geology

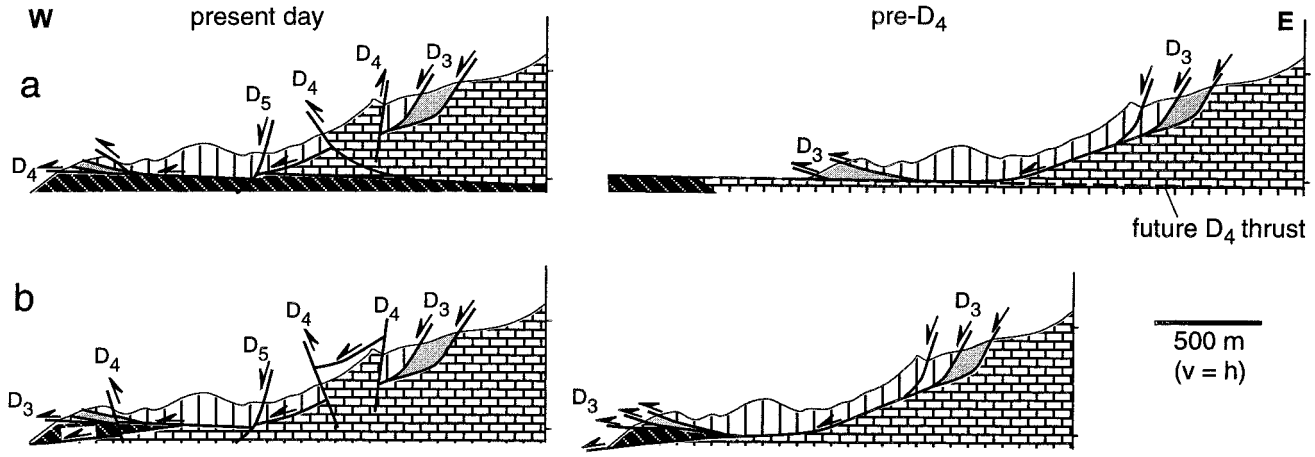

Fig. 17. (a) and (b) Schematic cross-sections illustrating different interpretations of how cataclastic shear zones at the base of the Kallithea nappe and on top of Katavasis complex might relate. The cross-sections on the left-hand side show the interpreted present-day geometry whereas the cross-sections on the right show the pre-D_4 geometry. Geometric relationships demand that offset along D_4 thrust in (a) must have been at least 3 km. Patterns as in Fig. 2. As discussed in text, we favour interpretation (b).

(Jacobshagen, 1986). (2) The cross-section in Fig. 17(b) is an alternative explanation in which both cataclastic shear zones link up. The knife-sharp fault on top of the Katavasis complex would be a splay of the underlying D_3 Kallithea detachment. Consequently this detachment system, and therefore the emplacement of the Kallithea nappe, would be < 10 Ma. This interpretation allows us to treat the Kallithea nappe and the Katavasis complex as one paleogeographic entity before emplacement onto the Kerketas nappe and the Cycladic blueschist unit. It would also give this entity an originally internal position, which is compatible with regional geologic constraints. Therefore, we envision scenario (2) to be more realistic. However, the late-D_3 emplacement of the Kallithea nappe and the Katavasis complex between 9 and 10 Ma (the lower age limit for the Kallithea detachment is given by the maximum age for D_4, see below) was top-to-the-NW/NNW and therefore in a different direction as the general D_3 transport deep in the nappe pile.

The envisioned < 10 Ma emplacement of the Kallithea nappe took place when the rocks of the Cycladic blueschist unit had already reached the surface (clasts from the Agios Nikolaos, Ampelos and Selçuk nappes in the Serravallian Basal Conglomerate Formation). Therefore, the extensional emplacement of the Kallithea nappe did not aid exhumation of the Cycladic blueschist unit on Samos Island. Because no pebbles from the Kerketas nappe were observed as components in the Basal Conglomerate Formation, we infer that this tectonically deepest unit was not exposed in pre-Tortonian times and the Kallithea detachment might have played a role in its exhumation.

Deformation/metamorphism relationships indicate that some D_3 structures developed before the Early Miocene climax of M_3 and should therefore be Oligocene in age (see also below). Several lines of evidence suggest that D_3 continued into the Middle and Late Miocene: (1) the Serravallian onset of sedimentation in the graben, (2) the inferred emplacement of the Kallithea nappe between 9 and 10 Ma, (3) microprobe work which indicates that D_3 structures developed at and after the peak of Early Miocene greenschist-facies M_3 metamorphism, (4) the Aegean was subjected to pronounced regional crustal extension during the Miocene.

6.3. D_4 contraction and D_5 extension

D_4 and D_5 are characterized by faulting along moderate to steep faults, which may have caused limited block rotations across the island. Furthermore, the dip pattern of bedding in the vicinity of and away from faults in the graben sediments supplies a measure for the degree of reorientation during faulting. We are confident that the majority of D_4 and D_5 faults have not been rotated to any great degree after their formation. Consequently, D_4 results from horizontal crustal contraction and D_5 from horizontal crustal extension.

Based on the youngest age for the Hora Formation and the oldest age for the unconformably overlying Mytilini Formation, Weidmann et al. (1984) placed the D_4 event into the period between 9 and 8.6 Ma. However, since this unconformity did apparently not develop at the same time across the entire basin, the D_4 event might have lasted somewhat longer than 8.6 Ma. Contractional deformation caused a major change in the sedimentary facies pattern; deep lacustrine sediments of the Hora Formation were replaced by fluvial deposits of the Mytilini Formation

suggesting that contraction was associated with pronounced uplift. Despite a large component of coaxial deformation, the general tectonic transport during D_4 appears to be top-to-the-W. We believe that the presently E-dipping structural grain (Figs. 2, 4 and 5b) of Samos Island was caused by D_4 reverse faulting and west-vergent folding.

The structural relationships on the western side of the Mytilini graben at the north coast indicate that D_4 reverse faulting postdated graben formation. This and the relationship between ductile D_3 structures and graben formation in the Pyrgos area are thought to supply strong evidence against a transpressional origin of the Miocene graben on Samos Island.

In the latest Miocene, extensional deformation (D_5) revived and continues until the present. The pattern of S-dipping listric and planar normal faults in the southern half of the island and N-dipping faults in the northern half suggest that D_5 largely controlled the present-day topography. Therefore, we regard Samos Island as a tilted horst block within the Aegean Sea.

7. Discussion

7.1. Interpretation of P–T data and subduction-zone retreat

The shape of the *P–T* path in Fig. 6 illustrates a major change in the thermal structure at ~30–35 Ma. The onset of high-pressure metamorphism in Crete at about 25 Ma (Seidel et al., 1982) occurred afterwards. Thomson et al. (1998) estimated an age of 32–>36 Ma for the initiation of subduction in Crete. The present plate-convergence rate of Africa with respect to Eurasia is ~15 mm/a (Livermore et al., 1985), whereas the Aegean region is moving southward to Africa at a rate of 30–40 mm/a (Le Pichon et al., 1995). This results in subduction rates of ~50 mm/a at the modern Hellenic subduction zone. Assuming an average geometry of an accretionary wedge (basal décollement ~7°, Davis et al., 1983), and that the present subduction rates are largely representative for the last ~35 Ma, we would expect that subduction to a depth of ~35 km (as deduced from *P–T* data on Crete, Seidel et al., 1982) would have occurred in about 6–7 Ma. The latter data suggest that the high-pressure rocks of Crete started to subduct at about 31–32 Ma. We note that the estimates for the onset of subduction beneath Crete of Thomson et al. (1998), our crude estimate, and the change in the thermal profile in the Cyclades/Samos region at ~30–35 Ma are similar. We believe that this time marks the obstruction of subduction in the Cyclades and the retreat of the subduction zone towards the south. The distribution of Miocene high-pressure rocks (Fig. 1) suggests that the subducting slab retreated only in the region south of the Aegean Sea. Asthenospheric return flow associated with the southward retreat of the subduction zone may have facilitated the profound Miocene magmatism in the Cyclades which in turn may have caused the increased thermal profile and prograde M_3 metamorphism. Because extensional deformation is commonly linked in some fashion to the retreat of the subduction zone (Lister et al., 1984; Buick, 1991), horizontal crustal extension should have commenced in the Early Oligocene, i.e. at about 30–35 Ma. Structures due to crustal extension were indeed dated at 32–34 Ma by Raouzaios et al. (1996) from Sifnos Island.

However, a number of studies (Urai et al., 1990; Buick, 1991; Faure et al., 1991; Lee and Lister, 1992; Forster and Lister, 1999) showed pronounced Middle Miocene to Recent crustal extension (e.g. formation of Cretan Sea) which can be observed across the entire present-day arc. The onset of graben development across the Aegean largely coincides with the inception of the North Anatolian fault (Barka and Hancock, 1984) and the westward extrusion of Anatolia (Le Pichon et al., 1995). We concur with Le Pichon et al. (1995) that initial retreat of the Hellenic slab in the Oligocene and Early Miocene exerted a pull on Anatolia which subsequently controlled its lateral extrusion. We propose that the extruding Anatolian microplate in turn impinged on the Hellenic slab and caused a second phase of retreat of the Hellenic slab from a position underneath Crete to its present position north of the Libyan coast.

The present-day relative plate motion (Le Pichon et al., 1995) in the upper-plate behind the magmatic arc, i.e. in the Cyclades, is divergent indicating that the Cyclades are a continental rift. According to the flow-line modelling of retreating subduction zones by Garfunkel et al. (1986), the asthenospheric flow in the arc and back-arc region behind retreating slabs is forced to accelerate in the horizontal to fill the free space causing plate divergence (rifting) (Fig. 18). We speculate that this process probably was and still is the

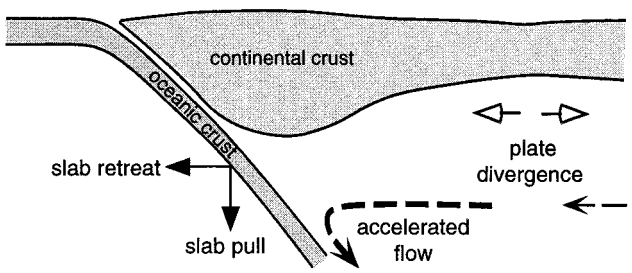

Fig. 18. Simplified sketch showing accelerated corner flow in the asthenosphere behind retreating subduction zone causing relative plate divergence in the back-arc area.

dominant cause for extending the upper plate in the Aegean.

7.2. Differential crustal extension during D_3

D_3 was characterized by a large degree of vertical shortening which might have caused the variable senses of shear within the Ampelos nappe. Nonetheless, the two pre-10 Ma D_3 shear zones, which overprinted the Pythagoras and Selçuk thrusts, had a relatively uniform top-to-the-ENE sense of shear. We propose that the simplest interpretation of the D_3 movement pattern is that these two D_3 shear zones are the main structures along which crustal-scale extension was localized. We interpret the D_3 kinematic indicators to reflect, in general, top-to-the-ENE tectonic transport. This transport direction for extensional deformation is in marked contrast to the uniform NNE–SSW-trending transport in the Cyclades and in the Menderes Massif of western Turkey. As shown above, both regions underwent considerably different degrees of crustal stretching. Consequently, a NNE-trending sinistral wrench corridor that accommodated differential crustal extension should have separated the Cyclades and the Menderes Massif (Fig. 19).

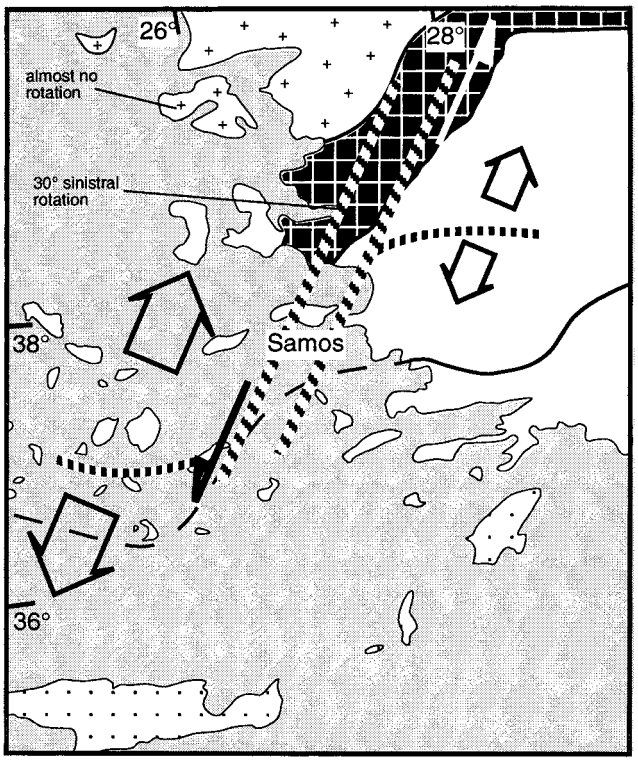

Fig. 19. Proposed sinistral wrench corridor, which is thought to have accommodated differential extension between the Cyclades and western Turkey. Paleomagnetically determined rotations from Kissel and Laj (1988) are indicated. Vertically ruled line separates areas of top-to-the-N and top-to-the-S sense of shear during crustal extension in the Aegean and the Menderes Massif, respectively; note that this boundary has been sinistrally displaced by ~150 km and that the Vardar–Izmir–Ankara suture is bent to the south.

We propose that this wrench corridor largely controlled D_3 extension in Samos. The local direction of extension in such a sinistral wrench corridor would be ENE; however, during ongoing deformation early formed stretching lineations would rotate anticlockwise and would finally occupy a similar orientation as those in the Cyclades and the Menderes Massif. The Miocene paleomagnetic rotations of about 30° reported by Kissel and Laj (1988) might have been caused in this wrench corridor. Bartley and Glazner (1991) and Janecke et al. (1991) have reported similar patterns of rotation in displacement transfer zones within extensional belts. We envision that differential extension was caused by the localized subduction-zone retreat in the Aegean which eventually created the Aegean Sea and the Hellenic arc.

If our interpretation of the existence of a sinistral wrench corridor was correct, it would lend strong support into a transtensional origin of the Miocene graben on Samos Island. The rapid subsidence recorded by the relatively thick section of the Hora Formation, the pronounced lateral facies changes from shallow to deeper lacustrine conditions recorded by the Pythagorion and Hora Formations and the difference in the occurrence of the unconformity are typical features of pull-apart basins (Christie-Blick and Biddle, 1985).

8. Conclusions

We reached the following conclusions:

1. Five generations of structures (D_1–D_5) have been recognized on Samos Island. D_3 caused the dominant regional deformation. D_2, D_3 and D_5 caused attenuation of the tectonostratigraphic pile.
2. $D_{1/2}$ structures caused nappe stacking and were subsequently highly overprinted. Therefore the kinematics of early nappe stacking remains controversial.
3. D_3 crustal extension commenced in the Early Oligocene and is largely coeval with a marked change in the thermal structure. We propose that this change in the thermal structure coincided with the retreat of the subduction zone towards the external Hellenides. The emplacement of the Kallithea nappe as part of the Cycladic ophiolite nappe occurred during the final stages of D_3 crustal extension between 9 and 10 Ma. In general, tectonic transport in the deep parts of the nappe pile was top-to-the-ENE, whereas the late, shallow-level emplacement of the Kallithea nappe was top-to-the-NW/NNW directed.

4. The geometry of pre-10 Ma D_3 extension contrasts with ~N–S extension in the neighbouring regions and might have been controlled by a sinistral wrench corridor that accommodated differential crustal extension between the Cyclades and the Menderes Massif.
5. D_4 contraction was a short-lived event, which caused local inversion of the Miocene graben. The cause of this event remains unknown.
6. After the Upper Tortonian, extensional deformation (D_5) revived and continues until the present. D_5 extension produced W/NW-striking faults that largely control the present-day geomorphology of the island.

Acknowledgements

Funded by the Deutsche Forschungsgemeinschaft (grants Ri 538/4-1 and Ri 538/4-2). We are particularly indebted to dozens of students from Mainz University who mapped the island of Samos in the course of various mapping projects. Their detailed work helped considerably to sort out details of the regional geology and overprinting relationships that were invaluable for the success of this study. C. Passchier, W. Lackmann, T. Güngör, K. Gessner, A. Willner and M. Okrusch contributed by discussions and/or technical assistance. Critical and detailed reviews by the journal referees John Bartley and Paul Williams were particularly helpful.

References

Altherr, R., Seidel, E. 1977. Speculations on the geodynamic evolution of the Attic–Cycladic crystalline complex during alpidic times. In: Kallergis, G. (Ed.), Geology of the Aegean Region, Proceedings, VI Colloquium, Athens. Institute of Geology and Mineral Exploration, pp. 347–351.

Altherr, R., Kreuzer, H., Wendt, I., Lenz, H., Wagner, G.H., Keller, J., Harre, W., Höhndorf, A., 1982. A late Oligocene/early Miocene high temperature belt in the Attic–Cycladic crystalline complex (SE Pelagonian, Greece). Geologisches Jahrbuch E23, 97–164.

Avigad, D., Garfunkel, Z., 1991. Uplift and exhumation of high-pressure metamorphic terrains: the example of the Cycladic blueschist belt (Aegean Sea). Tectonophysics 188, 357–372.

Avigad, D., Garfunkel, Z., Jolivet, L., Azanon, J.M., 1997. Back arc extension and denudation of Mediterranean eclogites. Tectonics 16, 924–941.

Barka, A., Hancock, P., 1984. Neotectonic deformation patterns in the convex northwards arc of the North Anatolian fault. In: Dixon, J.E., Robertson, A.H.F. (Eds.), The Geological Evolution of the Eastern Mediterranean. Geological Society of London Special Publication 17, pp. 529–536.

Bartley, J.M., Glazner, A.F., 1991. En échelon Miocene rifting in the southwestern United States and model for vertical-axis rotation in continental extension. Geology 19, 1165–1168.

Böger, H., 1988. Stratigraphische und tektonische Verknüpfungen kontinentaler Sedimente des Neogens im Ägäis-Raum. Geologische Rundschau 72, 771–814.

Boronkay, K., Doutsos, T., 1994. Transpression and transtension within different structural levels in the central Aegean region. Journal of Structural Geology 16, 1555–1573.

Bröcker, M., Kreuzer, H., Matthews, A., Okrusch, M., 1993. $^{40}Ar/^{39}Ar$ and oxygen isotope studies of polymetamorphism from Tinos Island, Cycladic blueschist belt, Greece. Journal of Metamorphic Geology 11, 223–240.

Bröcker, M., Enders, M., 1999. U–Pb zircon geochronology of unusual eclogite-facies rocks from Syras and Tinos (Cyclades, Greece). Geological Magazine 136, 111–118.

Buick, I.S., 1991. The late-Alpine evolution of an extensional shear zone, Naxos, Greece. Journal of the Geological Society of London 152, 639–654.

Candan, O., Dora, Ö.O., Oberhänsli, R., Oelsner, F., Dürr, S., 1997. Blueschist relics in the Mesozoic cover series of the Menderes Massif and correlations with Samos Island, Cyclades. Schweizerische Mineralogische und Petrographische Mitteilungen 77, 95–99.

Chen, G., Okrusch, M., Sauerschell, W., 1995. Polymetamorphic evolution of high-pressure rocks on Samos, Greece. In: Piskin, Ö., Ergün, M., Savascin, M.Y., Tarcan, G. (Eds.), International Earth Sciences Colloquium on the Aegean Region, Proceedings, Izmir, Turkey, pp. 359–365.

Chen, G., 1995. Evolution of the high- and medium-pressure metamorphic rocks on the island of Samos, Greece. Annales Géologiques des Pays Helléniques 36, 799–915.

Christie-Blick, N., Biddle, K.T., 1985. Deformation and basin formation along strike-slip faults. In: Biddle, K.T., Christie-Blick, N. (Eds.), Strike-slip Deformation, Basin Formation, and Sedimentation. Society of Economy, Paleontology and Mineralogy Special Publication 37, pp. 1–34.

Collins, A.S., Robertson, A.H.F., 1998. Processes of Late Cretaceous to Late Miocene episodic thrust sheet translation in the Lycian Taurides, SW Turkey. Journal of the Geological Society of London 155, 759–772.

Davis, D., Suppe, J., Dahlen, F.A., 1983. Mechanics of fold-and-thrust belts and accretionary wedges. Journal of Geophysical Research 88, 1153–1172.

Erdogan, B., Güngör, T., 1992. Menderes Masifi'nin kuzey kanadinin stratigrafisi ve tektonik evrimi. TPJD Bületeni 2, 1–20.

Fassoulas, C., Kilias, A., Mountrakis, D., 1994. Postnappe stacking extension and exhumation of high-pressure/low-temperature rocks in the island of Crete, Greece. Tectonics 13, 127–138.

Faure, M., Bonneau, M., Pons, J., 1991. Ductile deformation and syntectonic granite emplacement during the late Miocene extension of the Aegean (Greece). Geological Society of France Bulletin 162, 3–11.

Feehan, J.G., Brandon, M.T., 1999. Contribution of ductile flow to exhumation of low *T*–high *P* metamorphic rocks: San Juan–Cascade nappes, NW Washington State. Journal of Geophysical Research B104, 10883–10901.

Forster, M., Lister, G.S., 1999. Detachment faults in the Aegean core complex of Ios, Cyclades, Greece. In: Ring, U., Brandon, M.T., Lister, G.S., Willett, S.D. (Eds.), Exhumation Processes: Normal Faulting, Ductile Flow and Erosion. Special Publication of the Geological Society of London 154, 305–324.

Garfunkel, Z., Anderson, C.A., Schubert, G., 1986. Mantle circulation and the lateral migration of subducted slabs. Journal of Geophysical Research 91, 7205–7223.

Gautier, P., Brun, J.P., Jolivet, L., 1993. Structure and kinematics of Upper Cenozoic extensional detachment on Naxos and Paros (Cyclades islands). Tectonics 12, 1180–1194.

Ghosh, S.K., Ramberg, H., 1976. Reorientation of inclusions by combination of pure shear and simple shear. Tectonophysics 34, 1–70.

Hetzel, R., Ring, U., Akal, C., Troesch, M., 1995. Miocene NNE-directed extensional unroofing in the Menderes Massif, southwestern Turkey. Journal of the Geological Society of London 152, 639–654.

Jacobshagen, V., 1986. Geologie von Griechenland. Gebrüder Bornträger, Berlin 363 pp.

Janecke, S.U., Geissman, J.W., Bruhn, R.L., 1991. Localized rotation during Paleogene extension in east central Idaho: Paleomagnetic and geologic evidence. Tectonics 10, 403–432.

Jeffery, G.B., 1922. The motion of ellipsoidal particles immersed in a viscous fluid. Proceedings of the Royal Society of London A102, 161–179.

Kissel, C., Laj, C., 1988. The Tertiary geodynamical evolution of the Aegean arc: a paleomagnetic reconstruction. Tectonophysics 146, 183–201.

Kretz, R., 1983. Symbols for rock-forming minerals. American Mineralogist 68, 277–279.

Le Pichon, X., Angelier, J., 1979. The Hellenic arc and trench system: A key to the neotectonic evolution of the Eastern Mediterranean area. Tectonophysics 60, 1–42.

Le Pichon, X., Chamot-Rooke, N., Lallemant, S., Noomen, R., Veis, G., 1995. Geodetic determination of the kinematics of central Greece with respect to Europe: Implications for eastern Mediterranean tectonics. Journal of Geophysical Research B100, 12675–12690.

Lee, J., Lister, G.S., 1992. Late Miocene ductile extension and detachment faulting, Mykonos, Greece. Geology 20, 121–124.

Lister, G.S., Davis, G.A., 1989. The origin of metamorphic core complexes and detachment faults formed during continental extension in the northern Colorado River region, U.S.A. Journal of Structural Geology 11, 65–94.

Lister, G.S., Forster, M., 1996. Inside the Aegean metamorphic core complexes. Technical Publication Australian Crustal Research Centre 45, 110 pp.

Lister, G.S., Raouzaios, A., 1996. The tectonic significance of a porphyroblastic blueschist facies overprint during Alpine orogenesis, Sifnos, Aegean Sea, Greece. Journal of Structural Geology 18, 1417–1435.

Lister, G.S., Banga, G., Feenstra, A., 1984. Metamorphic core complexes of Cordilleran type in the Cyclades, Aegean Sea, Greece. Geology 12, 221–225.

Livermore, R.A., Smith, A.G., 1985. Some boundary conditions for the evolution of the Mediterranean region. In: Stanley, D.J., Wezel, F.-C. (Eds.), Geophysical Evolution of the Mediterranean Basins. Springer, Berlin, pp. 83–98.

Makris, J., Stobbe, C., 1984. Physical properties and state of the crust and upper mantle of the Eastern Mediterranean Sea deduced from geophysical data. Marine Geology 55, 347–363.

Massonne, H.-J., 1995. Experimental and petrogenetic study of UHPM. In: Coleman, R.G., Wang, X. (Eds.), Ultrahigh Pressure Metamorphism. Cambridge University Press, Cambridge, pp. 33–95.

Mezger, K., Okrusch, M., 1985. Metamorphism of a varigated sequence at Kallithea, Samos, Greece. Tschermaks Mineralogische und Petrographische Mitteilungen 34, 67–82.

Mposkos, E., Perdikatsis, V., 1984. Petrology of glaucophane metagabbros and related rocks from Samos, Aegean Island (Greece). Neues Jahrbuch Mineralogische Abhandlung 149, 43–63.

Mposkos, E., 1978. Diasporit- und Smirgelvorkommen der Insel Samos (Griechenland). Fourth International Congress for the Study of Bauxites 2, 614–631.

Okay, A.Ï., 1989. Geology of the Menderes Massif and the Lycian nappes south of Denizli, western Taurides. Bulletin of Mineral Research and Exploration 109, 37–51.

Okrusch, M., Bröcker, M., 1990. Eclogites associated with high-grade blueschists in the Cyclades archipelago, Greece: A review. European Journal of Mineralogy 2, 451–478.

Okrusch, M., Richter, P., Katsikatsos, G., 1984. High-pressure rocks of Samos, Greece. In: Dixon, J.E., Robertson, A.H.F. (Eds.), The Geological Evolution of the Eastern Mediterranean. Geological Society of London Special Publication 17, pp. 529–536.

Papanikolaou, D., 1979. Unités tectoniques et phases de déformation dans l'île de Samos, Mer Egée, Grèce. Geological Society of France Bulletin 21, 745–752.

Passchier, C.W., 1987. Stable positions of rigid objects in non-coaxial flow—a study in vorticity analysis. Journal of Structural Geology 9, 679–690.

Raouzaios, A., Lister, G.S., Foster, D.A., 1996. Oligocene exhumation and metamorphism of eclogite–blueschists from the island Sifnos, Cyclades, Greece. Geological Society of Australia Abstracts 41, 358.

Reinecke, T., 1982. Remnants of a Late Cretaceous high temperature belt on the Island of Anafi (Cyclades, Greece). Neues Jahrbuch Mineralogische Abhandlung 145, 157–182.

Ridley, J., 1984. The significance of deformation associated with blueschist-facies metamorphism on the Aegean island of Syros. In: Dixon, J.E., Robertson, A.H.F. (Eds.), The Geological Evolution of the Eastern Mediterranean. Geological Society of London Special Publication 17, pp. 545–550.

Ring, U., Brandon, M.T., 1994. Kinematic data for the Coast Range fault and implications for exhumation of the Franciscan subduction complex. Geology 22, 735–738.

Ring, U., Brandon, M.T., 1999. Ductile strain and mass loss in the Franciscan subduction complex: implications for exhumation processes in accretionary wedges. In: Ring, U., Brandon, M.T., Lister, G.S., Willett, S.D. (Eds.), Exhumation Processes: Normal Faulting, Ductile Flow and Erosion. Geological Society of London Special Publication 154, 55–86.

Ring, U., Gessner, K., Güngör, T., Passchier, C.W., 1999. The Menderes Massif of western Turkey and the Cycladic Massif in the Aegean—do they really correlate? Journal of the Geological Society of London 156, 3–6.

Ring, U., 1995. Horizontal contraction or horizontal extension: Heterogeneous Late Eocene and Early Oligocene general shearing during blueschist and greenschist facies metamorphism at the Pennine–Austroalpine boundary zone in the Western Alps. Geologische Rundschau 84, 843–859.

Ring, U., 1998. Exhumation of blueschists from Samos Island. Geological Society of Greece Bulletin 32, 97–104.

Rutter, E.H., Maddock, R.H., Hall, S.H., White, S.H., 1986. Comparative microstructures of natural and experimentally produced clay-bearing fault gouges. Pure and Applied Geophysics 124, 3–30.

Seidel, E., Kreuzer, H., Harre, W., 1982. A Late Oligocene/Early Miocene high pressure belt in the External Hellenides. Geologisches Jahrbuch E23, 165–206.

Seyitoglu, G., Scott, B.C., Rundle, C.C., 1992. Timing of Cenozoic extensional tectonic in west Turkey. Journal of the Geological Society of London 149, 533–538.

Theodoropoulos, D., 1979. Geological map of Greece, 1:50000, Samos Island: I.G.M.E., Athens.

Theye, T., Seidel, E., Vidal, O., 1992. Carpholite, sudoite, and chloritoid in low-grade high-pressure metapelites from Crete and the Peleponnese, Greece. European Journal of Mineralogy 4, 487–507.

Thomson, S.N., Stöckhert, B., Brix, M.A., 1998. Thermochronology of the high-pressure metamorphic rocks of Crete, Greece: Implications for the speed of tectonic processes. Geology 26, 259–262.

Thomson, S.N., Stöckhert, B., Brix, M.A., 1999. Miocene high-pressure metamorphic rocks of Crete, Greece: rapid exhumation by buoyant escape. In: Ring, U., Brandon, M.T., Lister, G.S., Willett, S.D. (Eds.), Exhumation Processes: Normal Faulting, Ductile Flow and Erosion. Geological Society of London Special Publication 154, 87–108.

Urai, J.L., Schuiling, R.D., Jansen, J.B.H., 1990. Alpine deformation on Naxos (Greece). In: Knipe, R.J., Rutter, E.H. (Eds.), Deformation Mechanisms, Rheology and Tectonics. Geological Society of London Special Publication 54, pp. 509–522.

Vandenberg, L.C., Lister, G.S., 1996. Structural analysis of basement tectonites from the Aegean metamorphic core complex of Ios, Cyclades, Greece. Journal of Structural Geology 18, 1437–1454.

Wallis, S.R., Platt, J.P., Knott, S.D., 1993. Recognition of syn-convergence extension in accretionary wedges with examples from the Calabrian arc and the Eastern Alps. American Journal of Science 293, 463–495.

Weidmann, M., Solounias, N., Drake, R.E., Curtis, G.H., 1984. Neogene stratigraphy of the eastern basin, Samos island, Greece. Geobios 17, 477–490.

Wheeler, J., Butler, R.W.H., 1994. Criteria for identifying structures related to true crustal extension in orogens. Journal of Structural Geology 16, 1023–1027.

Wijbrans, J.R., McDougall, I., 1988. Metamorphic evolution of the Attic Cycladic metamorphic belt on Naxos (Cyclades, Greece) utilizing $^{40}Ar/^{39}Ar$ age spectrum measurements. Journal of Metamorphic Geology 6, 571–594.

Wijbrans, J.R., Schliestedt, M., York, D., 1990. Single grain argon laser probe dating of phengites from the blueschist to greenschist transition on Sifnos (Cyclades, Greece). Contributions to Mineralogy and Petrology 104, 582–593.

Will, T., Okrusch, M., Schmädicke, E., Chen, G., 1998. Phase relations in the greenschist–blueschist–amphibolite–eclogite facies in the system Na_2O–CaO–FeO–MgO–Al_2O_3–SiO_2–H_2O (NCFMASH), with application to metamorphic rocks from Samos, Greece. Contributions to Mineralogy and Petrology 32, 85–102.